Interface focus

J. R. Soc. Interface (2009) **6**, S59–S81
doi:10.1098/rsif.2008.0381.focus
Published online 26 November 2008

A quantitative protocol for dynamic measurements of protein interactions by Förster resonance energy transfer-sensitized fluorescence emission

A. D. Elder[1], A. Domin[1], G. S. Kaminski Schierle[1], C. Lindon[2], J. Pines[3], A. Esposito[1] and C. F. Kaminski[1,4,*]

[1]*Department of Chemical Engineering and Biotechnology, University of Cambridge, Pembroke Street, Cambridge CB2 3RA, UK*
[2]*Department of Genetics, University of Cambridge, Downing Street, Cambridge CB2 3EH, UK*
[3]*Wellcome Trust/Cancer Research UK Gurdon Institute, The Henry Wellcome Building of Cancer and Developmental Biology, University of Cambridge, Tennis Court Road, Cambridge CB2 1QN, UK*
[4]*SAOT School of Advanced Optical Technologies, Max–Planck-Research Group, Division III, University of Erlangen-Nuremberg, Günther-Scharowsky-Strasse 1, Bau 24, 91058 Erlangen, Germany*

Fluorescence detection of acceptor molecules sensitized by Förster resonance energy transfer (FRET) is a powerful method to study protein interactions in living cells. The method requires correction for donor spectral bleed-through and acceptor cross-excitation as well as the correct normalization of signals to account for varying fluorophore concentrations and imaging parameters. In this paper, we review different methods for FRET signal normalization and then present a rigorous model for sensitized emission measurements, which is both intuitive to understand and practical to apply. The method is validated by comparison with the acceptor photobleaching and donor lifetime-imaging techniques in live cell samples containing EYFP and ECFP tandem constructs exhibiting known amounts of FRET. By varying the stoichiometry of interaction in a controlled fashion, we show that information on the fractions of interacting donors and acceptors can be recovered. Furthermore, the method is tested by performing measurements on different microscopy platforms in both widefield and confocal imaging modes to show that signals recovered under different imaging conditions are in quantitative agreement. Finally, the method is applied in the study of dynamic interactions in the cyclin–cdk family of proteins in live cells. By normalizing the obtained signals for both acceptor and donor concentrations and using a FRET exhibiting control construct for calibration, stoichiometric changes in these interactions could be visualized in real time. The paper is written to be of practical use to researchers interested in performing sensitized emission measurements. The correct interpretation of the retrieved signals in a biological context is emphasized, and guidelines are given for the practical application of the developed algorithms.

Keywords: FRET; sensitized emission; microscopy; FLIM

1. INTRODUCTION

Förster resonance energy transfer (FRET) refers to the transfer of energy from a donor fluorophore to an acceptor, which occurs if the emission spectrum of the donor exhibits overlap with the absorption spectrum of the acceptor. If the acceptor is also a fluorophore, then FRET leads to an increase in fluorescence emission from the acceptor, and this is referred to as sensitized emission. The term 'fluorescence resonance energy transfer' is frequently used in the literature to describe this phenomenon, which is possibly misleading, since FRET is not mediated by the emission of photons (fluorescence) from the donor. Evidence for FRET was found more than 80 years ago (Cario & Franck 1922) and

*Author for correspondence (cfk23@cam.ac.uk).

Electronic supplementary material is available at http://dx.doi.org/10.1098/rsif.2008.0381.focus or via http://journals.royalsociety.org.

One contribution of 9 to a Theme Supplement 'Quantitative fluorescence microscopy: The 1st international Theodor Förster lecture series'.

Received 3 September 2008
Accepted 3 November 2008

the process was recognized to arise from a long range dipole–dipole interaction (Perrin 1927, 1932). The first theory that could quantitatively describe the process was, however, developed by Theodor Förster and presented in his seminal paper from 1948 (Förster 1948*b*). In contrast to earlier scientists, he recognized that, for significant FRET to occur, donor and acceptor molecules need to be within a distance of less than approximately 10 nm, with the efficiency of energy transfer decreasing rapidly with separation. It is this latter property that has made FRET one of the most useful and widely applied tools in use today to measure distances on the molecular scale (Stryer 1978; Lakowicz 2006). One of the most exciting and most rapidly growing fields of FRET application is microscopic imaging in living cells (Selvin 2000; Wouters *et al.* 2001). For in-depth reviews on FRET imaging, see Pollok & Heim (1999), Jares-Erijman & Jovin (2003, 2006), Miyawaki (2003), Periasamy & Day (2005), Van Munster *et al.* (2005) and Wallrabe & Periasamy (2005). This burgeoning field has been enabled through the discovery and maturation of fluorescent fusion protein (FP) technology permitting interaction partners to be fluorescently labelled and detected with the required specificity and sensitivity at excitation and emission wavelengths compatible with FRET (Shaner *et al.* 2005; Giepmans *et al.* 2006; Shu *et al.* 2006). A popular approach for detecting FRET is fluorescence lifetime-imaging microscopy (FLIM). Usually this is performed by monitoring the decrease in the lifetime of donor molecules in the presence of FRET although other approaches are possible. FLIM has been combined with powerful data-fitting algorithms and data representation approaches including global analysis and phasor plots (e.g. Verveer *et al.* 2000; Clayton *et al.* 2004; Pelet *et al.* 2004; Digman *et al.* 2008). Where measurement speed and low signal levels are not an issue, FLIM is often the most straightforward method for the verification of FRET interactions.

For dynamic live cell FRET applications, the sensitized emission measurement is the most widely used approach (Erickson *et al.* 2001; Zal & Gascoigne 2004) and this is the focus of the present paper. The method can be implemented on standard confocal and widefield microsopes. Its non-destructive nature (in contrast to the popular acceptor photobleaching technique) and sensitivity even at high acquisition speed (in contrast to fluorescence lifetime imaging; Kölner & Wolfrum 1992) make it the method of choice for measurements over extended periods of time. These advantages are, however, offset by the fact that quantification of FRET by measuring sensitized emission is extremely difficult in practice. Imperfections in the spectral properties of fluorophores used in live cell FRET experiments lead to the problem of signal crosstalk that contaminates the FRET signal (Tron *et al.* 1984; Youvan *et al.* 1997; Gordon *et al.* 1998; Nagy *et al.* 1998; Xia & Liu 2001; Elangovan *et al.* 2003). The most serious issue, and the most difficult to quantify, relates to the fact that not all donors and acceptors participate in FRET interactions and the signals need to be normalized to take into account the varying concentrations of participating interaction partners (Clegg 1995; Hoppe *et al.* 2002; Berney & Danuser 2003; Gu *et al.* 2004; Millington *et al.* 2007; Wlodarczyk *et al.* 2008). This is a severe challenge as expression levels of FPs in live cells may vary greatly in space and in time. However, neglecting these effects can lead to false conclusions, and one may not even be able to establish whether two proteins interact or not. Furthermore, the biological interaction one wishes to track may change stoichiometry, i.e. the relative fractions of tagged proteins participating in the interaction are changing in time. Correct signal normalization is crucial to reliably detect and quantify such changes.

A number of publications have appeared in the literature to deal with crosstalk correction and signal normalization. A number of different notations are used, and there are subtle differences in the way normalizations are performed. This makes selection of the most appropriate method a daunting task even for experienced microscopists. In this paper, we aim to address these issues. We begin with an extensive review of existing normalization methods, and then present an intuitive, yet rigorous, model for sensitized emission FRET, which is appropriate for most applications in living cells. The various normalization methods are interpreted in a practical context. We validate the developed algorithms using control constructs exhibiting known amounts of FRET, and show, by controlled perturbation of the interaction stoichiometry, that information on the fractions of interacting partners can be retrieved. We validate the method against other measures of FRET quantification, namely the acceptor photobleaching method and FLIM. Our method yields quantities that are system independent, such that experiments obtained with different systems are directly comparable. This latter step is crucial as different algorithms can yield FRET efficiencies that differ very significantly in value making the verification of experiments performed by others a difficult task; a point that has often been neglected in the literature. We verify explicitly that FRET data we measure from similar constructs but using different imaging platforms agree quantitatively. Finally, we apply the methodology for the *in vivo* quantification of dynamic protein–protein interactions. We track interactions of the cyclin–cdk family of proteins throughout the cell cycle in real time. We show that normalizing FRET signals for both the acceptor and donor concentrations permits changes in the interaction stoichiometry of the binding proteins to be followed in time, offering maximal information from a given experiment. Algorithms developed here have been incorporated in user-friendly image analysis software, which is published online and freely available to the interested user at http://laser.ceb.cam.ac.uk.

2. BACKGROUND

2.1. Förster resonance energy transfer

In what follows, we assume that both donor and acceptor molecules are fluorescing species, as is usual for sensitized emission measurements. The rate of energy transfer, $k_T(r)$, from an excited donor to an acceptor

molecule is given by (Clegg 1996; Lakowicz 1999)

$$k_{\mathrm{T}}(r) = \frac{1}{\tau_{\mathrm{D}}}\left(\frac{R_0}{r}\right)^6, \tag{2.1}$$

where τ_{D} is the donor lifetime; r is the separation distance; and R_0 is the Förster radius, defined as the interfluorophore distance at which the FRET efficiency is 50 per cent.

The FRET transfer efficiency, E, is defined as the fraction of energy absorbed by the donor that is transferred to the acceptor

$$E = \frac{k_{\mathrm{T}}}{k_{\mathrm{T}} + {\tau_{\mathrm{D}}}^{-1}} = \frac{{R_0}^6}{{R_0}^6 + r^6}. \tag{2.2}$$

R_0 is often assumed to be a constant for a given pair of fluorophores. In reality, it is a function of the donor quantum yield, the refractive index of the medium through which the signals propagate and the orientation factor, κ^2, between the donor and acceptor dipole moments (Van Der Meer 2002), all of which may vary in time and in space within a living cell (Lakowicz 1999; Jares-Erijman & Jovin 2003). For a theoretical derivation of R_0 and equation (2.1), the reader is referred to the excellent original paper by Förster (1948*a*) and the in-depth review by Clegg (1996).

2.2. FRET quantification methods

Three methods are commonly used for FRET quantification, namely measurement of sensitized emission, photobleaching and lifetime imaging. Although the focus here is on sensitized emission, we present measurements of, and comparison with, photobleaching and lifetime measurement techniques, and a brief introduction to each of the three methods is given in the following sections. Note that other methods have also been demonstrated for FRET determination, for example polarization measurements (Jares-Erijman & Jovin 2003; Rizzo & Piston 2005).

2.2.1. Sensitized emission. Crosstalk. The sensitized emission technique quantifies FRET by measuring the increase in acceptor emission upon energy transfer from the donor. This is traditionally measured using a 'FRET filter set', consisting of an excitation bandpass designed to selectively excite the donor and an emission window designed to selectively collect acceptor emission. The excitation bandpass is referred to as 'donor excitation' and the emission bandpass is referred to as the 'acceptor channel'. Theoretically this FRET filter set directly measures the amount of FRET in a sample. In reality, however, spectral bleed-through (donor fluorophore emission into the acceptor channel) and cross-excitation (direct excitation of acceptor fluorophores by donor excitation) contaminate the signal. This is referred to as crosstalk.

Figure 1 shows how cross-excitation (path 1) and spectral bleed-through (path 2) affect the measured FRET signals.

The problem of crosstalk is widely recognized in the literature, and many corrections for it have been proposed (Tron *et al.* 1984; Youvan *et al.* 1997; Gordon *et al.* 1998; Nagy *et al.* 1998; Elangovan *et al.* 2003).

Figure 1. Crosstalk in sensitized emission FRET measurements. With no crosstalk (paths 1 and 2 inactive), the only path to the acceptor channel is via FRET. When crosstalk is present (paths 1 and 2 active), contamination of the FRET signal occurs.

These approaches appear to be different because of different nomenclatures employed but they can be mathematically shown to be identical. The methods do however differ in the way that signal normalization is performed to account for concentration variations of interacting molecules (see §2.2.2).

Crosstalk is corrected for by performing two reference measurements in addition to the actual FRET experiment. One is performed using a control sample containing only donor fluorophores and the other on a sample containing only acceptor fluorophores. The former permits the bleed-through to be determined (path 2 in figure 1), whereas the latter is used in the determination of direct acceptor excitation. In the actual FRET experiment, this information is used to recover the true FRET contribution in the acceptor channel. In what follows, this is referred to as the corrected FRET signal, or cFRET.

Some methods also allow for bleed-through of acceptor signal into the donor channel and direct excitation of the donor by acceptor excitation (Gordon *et al.* 1998; Nagy *et al.* 1998). Note that this possibility is not included in the model of the FRET process depicted in figure 1: by careful selection of fluorophores, excitation filters and emission filters, the need for these corrections can usually be avoided, making the analysis inherently more robust because the accumulative error becomes smaller. The robustness of FRET algorithms due to noise across channels has been subject to a theoretical study by Neher & Neher (2004*b*).

2.2.2. Normalization methods. A key issue for FRET quantification is the normalization of the sensitized acceptor emission signal for fluorophore concentrations and equipment settings. Correct signal normalization is essential in order to allow quantitative comparisons to be made between experiments performed with varying instrument settings, on different microscopes and with different fluorophores. Many different approaches to FRET signal normalization have been described in the literature.

The measured FRET signal can be a function of donor concentration, acceptor concentration or both. The signal is also dependent on the fraction of donors and acceptors, which are within the proximity required for FRET. In a biological sample, this may depend on the stoichiometry of the interaction (e.g. what fraction of donor labelled protein A interacts with acceptor labelled protein B?).

Ideally, a normalization scheme is capable of quantifying FRET on an absolute scale, independent of these factors. The transfer efficiency, E, defined in equation (2.2), is useful in this respect as it measures

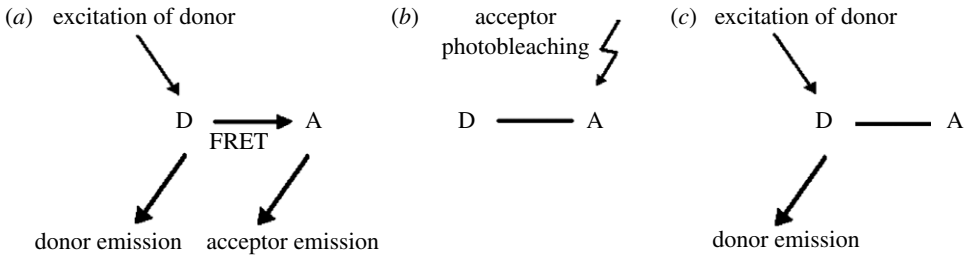

Figure 2. Diagram illustrating the acceptor photobleaching approach. (*a*) Before bleaching, the donor loses some energy due to FRET. (*b*) Bleaching results in photodestruction of the acceptor. (*c*) After bleaching, the donor emission is increased as the donor no longer loses energy via FRET.

the fractional energy absorbed by the donor that is transmitted to the acceptor.

The simplest approach to account for donor concentration is to divide cFRET by the unmixed donor signal (Vanderklish *et al.* 2000). However, the unmixed donor signal is *not* a direct measure of the donor concentration, because it is depleted when energy transfer to the acceptor takes place. Furthermore, the result is still system dependent and depends on excitation intensity, and detection efficiencies of the system used (Zal & Gascoigne 2004).

A similar method has been proposed to normalize the signal for acceptor concentration, namely the division of cFRET by the unmixed acceptor signal (Jiang & Sorkin 2002). Again the normalized signal cannot be compared across experiments where different fluorophores or excitation wavelengths are used, as it depends on the relative absorption strengths of the donor and acceptor fluorophores at the donor excitation wavelength used (Zal & Gascoigne 2004).

Gordon *et al.* (1998) proposed a normalization, FRETN, to account for both the donor and acceptor concentrations. To achieve this, cFRET is divided by the product of I^{DD} (the signal measured in the donor channel when using donor excitation) and I^{AA} (the signal measured in the acceptor channel when using acceptor excitation). However, it was later shown that the result of this normalization is still a function of concentration (Xia & Liu 2001; Zal & Gascoigne 2004). Xia & Liu (2001) suggest an alternative strategy in which the geometric mean of I^{DD} and I^{AA} is used to normalize cFRET. The signal is now no longer a function of concentration; however, the method fails to take into account the fact that the unmixed donor signal is not a direct measure of the donor concentration (because of depletion due to energy transfer) and the obtained signal is not directly proportional to the transfer efficiency. Also, this normalization procedure is again not independent of the system parameters.

The interpretation of the normalized FRET signals in terms of an absolute transfer efficiency E has been the subject of numerous previous publications. Under the assumption that each donor interacts with a single acceptor, E can be derived through a normalization by the unmixed donor signal if the loss due to energy transfer is also taken into account. In order to do this, the relative sensitivities of the two detection channels and the quantum yields of the donor and acceptor need to be known (Nagy *et al.* 1998; Elangovan *et al.* 2003; Wallrabe & Periasamy 2005) or determined from complementary acceptor photobleaching experiments (Van Rheenen *et al.* 2004; Zal & Gascoigne 2004). It is possible to relax the assumption that every donor interacts with an acceptor, through the introduction of a parameter representing the percentage of interacting donors, χ_D. Here, some methods calculate an apparent transfer efficiency represented by $\chi_D E$ (Elangovan *et al.* 2003; Zal & Gascoigne 2004; Wallrabe & Periasamy 2005).

In situations where one assumes that every acceptor fluorophore is interacting with a donor fluorophore (and there are surplus, non-interacting donors present), one can recover E via normalization of signals by the acceptor concentration. This is similar to acceptor normalization proposed by Jiang & Sorkin (2002), but requires inclusion of a corrective factor to account for the relative absorption strengths of the fluorophores (Nagy *et al.* 1998; Van Rheenen *et al.* 2004). In analogy to the previous example, the assumption that every acceptor interacts with a donor can be relaxed by the introduction of a parameter representing the percentage of interacting acceptors, χ_A.

A rigorous approach for the determination of FRET stoichiometry is published in Hoppe *et al.* (2002). A FRET exhibiting control construct is used, for which the stoichiometry of interaction between donors and acceptors is 1. This is then used to calibrate data obtained from FRET samples whose stoichiometry is not known. The idea of a FRET positive control construct is also central to the approach we present in this paper. An equivalent theoretical description is given in matrix form in Neher & Neher (2004*a*).

The method presented here is intuitive and practical to apply for measurement in biological samples and it incorporates all normalization methods reviewed earlier. Both the strength of interaction and information on the fractions of interacting partners can be recovered. Results are independent of the spectral parameters used for excitation and detection, and we show that measurements obtained on different equipment and using different systems can be directly compared.

Acceptor photobleaching. Photobleaching refers to the photodestruction of a fluorophore. Following photodestruction, a fluorophore will no longer absorb or emit fluorescence.

There are several different ways in which photobleaching can be used to measure FRET (Van Munster *et al.* 2005; Wlodarczyk *et al.* 2008). These can be split into ways that require a photostable donor and photolabile acceptor and vice versa. With a photostable

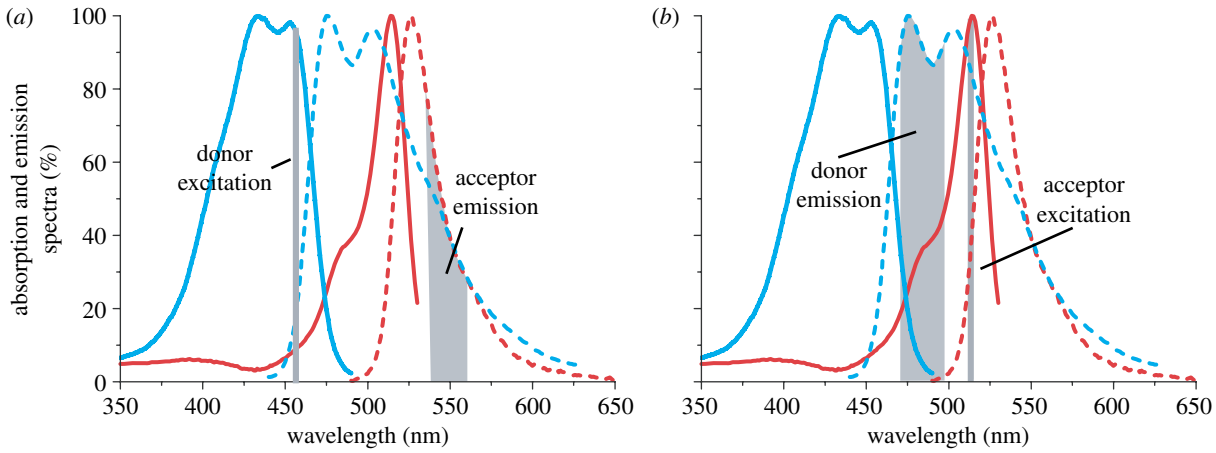

Figure 3. (*a*,*b*) Crosstalk in CFP–YFP FRET system. The excitation and emission wavelengths shown in light grey correspond to the settings on a confocal microscope used for the present work. The excitation wavelengths and emission spectral bandpasses are indicated in light grey and correspond to the parameters detailed in § 5.2 (see table 3). It is seen that donor bleed-through and direct acceptor excitation are significant. However, direct excitation of the donor at the acceptor excitation wavelength is negligible, as is acceptor emission into the donor emission channel. These characteristics justify the use of the model shown in figure 1. Red solid line, CFP absorption; red dashed line, CFP emission; blue solid line, YFP absorption; blue dashed line, YFP emission.

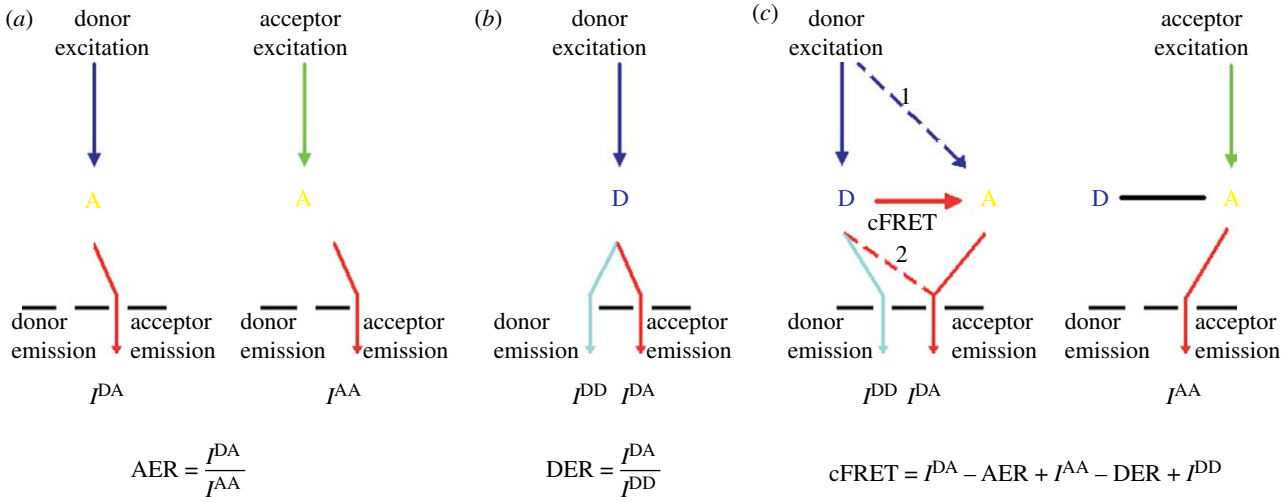

Figure 4. Diagram summarizing the principles behind the AER, DER and cFRET calculations. (*a*) The AER is determined from an acceptor-only sample. It is the ratio of emission into the acceptor channel when using donor excitation relative to when using acceptor excitation. (*b*) The DER is determined from a donor-only sample. It is the ratio of emission into the acceptor channel relative to emission into the donor channel, when using donor excitation. (*c*) The aim is to measure cFRET; however, this signal is contaminated by the signal from paths 1 (AER.I^{AA}) and 2 (DER.I^{DD}).

acceptor, donor bleaching can be used to distinguish sensitized acceptor fluorescence from directly excited acceptor fluorescence (Mekler 1994). With a photostable donor, photobleaching of the acceptor due to excitation via FRET (Mekler *et al.* 1997) or direct acceptor photobleaching (Wouters *et al.* 1998; Llopis *et al.* 2000; Chan *et al.* 2001; Kenworthy 2001; Gu *et al.* 2004) can be used to determine FRET. Direct acceptor photobleaching is the most commonly used approach, because it is the most straightforward method to interpret. All photobleaching methods rely on the basic principle of measuring fluorescence emission pre- and post-bleaching. This is shown in figure 2.

An inherent problem with photobleaching methods is the inadvertent bleaching of the 'photostable' fluorophore. Recently, a method has been proposed (Van Munster *et al.* 2005) which monitors donor and acceptor fluorescence as a function of time, while gradual photobleaching is carried out. By fitting a mono-exponential model of bleaching to the data, the FRET efficiency can be calculated. This overcomes the problem of accidental bleaching, but does prolong imaging time.

The fact that the FRET reporters are destroyed in the process makes the method unsuitable for time-lapse applications in living cells. Problems are also the inadvertent bleaching of the photostable fluorophore and the unknown phototoxic effects induced by photobleaching. It has recently been shown that YFP can photo-convert to a CFP-like molecule when bleached, which can cause false positive results (Valentin *et al.* 2005). In practice, bleaching of the acceptor will be neither homogeneous nor complete.

In the present work, the direct acceptor photobleaching technique is used to provide a secondary transfer efficiency measurement for comparison with the results of the developed sensitized emission technique.

Lifetime imaging. Many studies have used FLIM to show the presence of FRET, with measurements in both the time domain and frequency domain (Gadella & Jovin 1995; Ng *et al.* 1999; Haj *et al.* 2002; Calleja *et al.* 2003). The transfer efficiency can be determined from the lifetime of the donor fluorophore in the presence of the acceptor, τ, and the lifetime of the donor fluorophore in the absence of the acceptor, τ_0, as shown by equation (2.3) (Lakowicz 1999)

$$E = 1 - \frac{\tau}{\tau_0}. \tag{2.3}$$

Here, the donor lifetime-imaging technique is used for comparison with the developed sensitized emission technique. FRET can also be measured by observing the acceptor fluorophore lifetime or a combination of the donor and acceptor lifetimes. The latter is useful when fluorophores are spectrally indistinguishable (Harpur *et al.* 2001).

In reality, fluorophore decays are multi-exponential (Tramier *et al.* 2002) and so the true transfer efficiency cannot simply be calculated through an application of equation (2.3). In this situation, careful analysis of multi-exponential decays using time-correlated single photon counting (TCSPC) can yield more complete information on the problem than is available from other techniques (Duncan *et al.* 2004; Millington *et al.* 2007). However, TCSPC is not always suitable for cellular imaging because large numbers of photons are needed per pixel in order to accurately fit multi-exponential decays (Kölner & Wolfrum 1992). For multi-exponential decays, the average of measured lifetimes $\langle\tau\rangle$ is calculated (Lakowicz 1999) and used to determine the transfer efficiency (Hoppe *et al.* 2002; Grailhe *et al.* 2006),

$$E = 1 - \frac{\langle\tau\rangle}{\langle\tau_0\rangle}, \tag{2.4}$$

where $\langle\tau\rangle$ and $\langle\tau_0\rangle$ are the mean lifetimes in the presence and absence of FRET, respectively.

3. CROSSTALK CORRECTION OF FRET SIGNALS

Figure 1 shows two main causes for crosstalk: direct excitation of the acceptor at the donor excitation wavelength (path 1) and donor emission bleed-through into the acceptor detection channel (path 2). In what follows, we assume that the acceptor emission does not bleed-through to the donor detection channel and, furthermore, that there is no direct excitation of the donor at the acceptor excitation wavelength. This is consistent with what is observed for many popular fluorophore pairs used for FRET in biology, e.g. pairs of fluorescent proteins such as CFP/YFP (figure 3) and organic fluorophores such as Alexa-488/568, respectively.

By designing experiments not to require these additional corrections, FRET quantification becomes inherently more robust.

3.1. Correcting for direct acceptor excitation

In the following sections, we frequently refer to figure 4, which summarizes the principles for obtaining the unmixed FRET signals, cFRET. Signal due to direct excitation of acceptors at the donor excitation wavelength is quantified by the measurement of the acceptor excitation ratio, AER, from a control sample containing only acceptor fluorophores (figure 4*a*). This is the ratio of the signal I^{DA} (excitation at the donor excitation wavelength, detection by the acceptor emission channel) relative to the signal I^{AA} (signal upon excitation at the acceptor excitation wavelength and detection by the acceptor emission channel). In a real sample then, where one wishes to determine FRET levels (figure 4*c*), one obtains

$$\text{signal due to cross excitation (path 1)} = \mathrm{AER} I^{\mathrm{AA}}. \tag{3.1}$$

3.2. Correcting for donor bleed-through

The amount of donor bleed-through into the acceptor channel is accounted for in an analogous way from a measurement of a donor emission ratio (DER) obtained from a control sample containing only donors. Referring to figure 4*b*, one obtains

$$\text{signal due to path 2} = \mathrm{DER} I^{\mathrm{DD}}, \tag{3.2}$$

where I^{DD} is the emission in the donor channel upon donor excitation.

The analysis programs developed here compute the AER and DER on a pixel-by-pixel basis. Plots of AER or DER against signal intensity provide useful diagnostic information: ideally, the AER and DER are constants and do not dependent on the amplitude of observed signals. Strong deviations from this behaviour indicate potential problems, such as errors in the background correction scheme or nonlinearities of the detection system. For pixels with low signal levels, the probability for errors is increased as background, e.g. from autofluorescence, may become appreciable in comparison with the signal itself. Regions thus identified in an experiment can be excluded from analysis and appropriate thresholds set.

3.3. Corrected FRET

The corrected FRET signal cFRET from a real sample is now obtained using the AER and DER and measurement of I^{DA}, I^{AA} and I^{DD} on the FRET sample (figure 4*c*). Hence

$$\mathrm{cFRET} = I^{\mathrm{DA}} - \mathrm{DER} I^{\mathrm{DD}} - \mathrm{AER} I^{\mathrm{AA}}. \tag{3.3}$$

4. SIGNAL NORMALIZATION

For the sake of clarity, full derivations of the signal normalization equations presented in the following sections are given in appendix A and only results are stated here.

4.1. Donor concentration normalization

Here cFRET is normalized for the donor concentration in the sample under observation. The donor-normalized FRET signal is given by

$$\mathrm{dFRET} = \frac{N_{\mathrm{D}}^{*}}{N_{\mathrm{D}} + N_{\mathrm{D}}^{*}} E = \chi_{\mathrm{D}} E, \tag{4.1}$$

which calculates an apparent transfer efficiency representing the actual transfer efficiency, E, scaled by the fraction of donor molecules, which contributes to FRET. N_{D}^{*} are the donor molecules in FRET proximity to the acceptors and $N_{\mathrm{D}}^{*}+N_{\mathrm{D}}$ is the total number of donor molecules, including non-interacting ones. The term $\chi_{\mathrm{D}}=N_{\mathrm{D}}^{*}/(N_{\mathrm{D}}+N_{\mathrm{D}}^{*})$ represents the fraction of interacting donors (Erickson *et al.* 2001; Hoppe *et al.* 2002). We prove in appendix A that

$$\mathrm{dFRET}=\frac{\mathrm{cFRET}\,\frac{\alpha}{\mathrm{DER}}}{I^{\mathrm{DD}}+\mathrm{cFRET}\,\frac{\alpha}{\mathrm{DER}}}, \tag{4.2}$$

where we have introduced a system specific parameter α

$$\alpha=\frac{Q_{\mathrm{D}}\,T_{\mathrm{D}}^{\mathrm{A}}}{Q_{\mathrm{A}}\,T_{\mathrm{A}}^{\mathrm{A}}}, \tag{4.3}$$

which relates to the fluorescence quantum yields Q_{D} and Q_{A} of donors and acceptors, respectively, and the relative signal collection efficiencies $T_{\mathrm{D}}^{\mathrm{A}}/T_{\mathrm{A}}^{\mathrm{A}}$ of donor and acceptor photons, which are emitted into the acceptor channel. The latter depends on the emission line shapes of donors and acceptors and the overlap with the acceptor channel band pass (figure 3*a*). If these are known, α can be calculated. Alternatively, we show in §6.1 how α can be measured directly using control samples exhibiting a controlled amount of FRET. Importantly, α is a constant for a given fluorophore pair and detection channel and thus needs to be determined only once for a given system. Furthermore, α is independent of system gain and thus constant between experiments where the detector gain is adjusted. This is highly advantageous, as this increases the dynamic range over which one is able to conduct experiments (e.g. measuring both weak and strongly emitting samples).

dFRET determined as defined in (4.2) calculates a quantity that is absolute and which can thus be compared for measurements obtained from different microscope platforms with differing collection efficiencies, fluorophores, etc. and it takes into account that both interacting and non-interacting fluorophores may be present. In §6.2, we show how the quantity dFRET compares for experiments obtained in different laboratories with differing equipment, and how it responds to changes in FRET stoichiometry. Apart from α, which has to be determined once for a given system, equation (4.2) contains only quantities that are measurable using the procedures outlined in figure 4.

4.2. Acceptor concentration normalization

In a similar fashion, the acceptor-normalized FRET signals are obtained, given by

$$\mathrm{aFRET}=\frac{N_{\mathrm{D}}^{*}}{N_{\mathrm{A}}+N_{\mathrm{A}}^{*}}\,E=\chi_{\mathrm{A}}E, \tag{4.4}$$

which weights the actual transfer efficiency by the number of molecules involved in FRET relative to the total number of acceptor molecules. χ_{A} is the fraction of interacting to the total number of acceptor molecules (since $N_{\mathrm{D}}^{*}=N_{\mathrm{A}}^{*}$). We obtain (see appendix A)

$$\mathrm{aFRET}=\frac{\mathrm{cFRET}}{\mathrm{AER}I^{\mathrm{AA}}\beta}. \tag{4.5}$$

The unmixed FRET signal, cFRET, is divided by $\mathrm{AER}I^{\mathrm{AA}}$, which is proportional to the acceptor concentration as the donor is not excited by the acceptor excitation wavelength.

The parameter β is introduced to account for the relative absorption strengths of the donors and acceptors and is given by

$$\beta=\frac{\left(B_{\mathrm{D}}^{\mathrm{D}}\Gamma_{\mathrm{D}}^{\mathrm{D}}\right)}{\left(B_{\mathrm{A}}^{\mathrm{D}}\Gamma_{\mathrm{A}}^{\mathrm{D}}\right)}, \tag{4.6}$$

where $B_{\mathrm{D}}^{\mathrm{D}}$ and $B_{\mathrm{A}}^{\mathrm{D}}$ relate to the emission strengths of donors and acceptors, respectively, upon excitation at the donor wavelength; $\Gamma_{\mathrm{D}}^{\mathrm{D}}$ and $\Gamma_{\mathrm{A}}^{\mathrm{D}}$ are the spectral overlap factors of donors and acceptors at the donor excitation wavelength. The β can again be calculated if the spectral characteristics of the donor and acceptors are known, as well as the characteristics of the excitation source. If narrow linewidth excitation sources are used (e.g. laser sources), then β is simply the ratio of the extinction coefficients of the donor and the acceptor, both excited at the donor excitation wavelength (see figure 3*a*). If broadband sources are used (e.g. filtered white light sources), the overlap integrals $\Gamma_{\mathrm{D}}^{\mathrm{D}}$ and $\Gamma_{\mathrm{A}}^{\mathrm{D}}$ between the excitation sources and the absorption line shapes need to be calculated to obtain β.

An alternative is to use a positive FRET control construct with known FRET efficiency and stoichiometry to obtain β as will be demonstrated in §6.1. The acceptor-normalized FRET efficiency becomes system and detector gain independent.

4.3. Concentration geometric mean normalization

By combining equations (4.1), (4.2), (4.4) and (4.5), a normalization based on the geometric mean of donor and acceptor fluorophore concentrations can be defined,

$$\mathrm{geoFRET}=\frac{N_{\mathrm{D}}^{*}}{\sqrt{\left(N_{\mathrm{A}}+N_{\mathrm{A}}^{*}\right)\left(N_{\mathrm{D}}+N_{\mathrm{D}}^{*}\right)}}\,E, \tag{4.7}$$

$$\mathrm{geoFRET}=\frac{\mathrm{cFRET}}{\sqrt{\left(I^{\mathrm{AA}}\beta\mathrm{AER}\right)\left(I^{\mathrm{DD}}\,\frac{\mathrm{DER}}{\alpha}+\mathrm{cFRET}\right)}}. \tag{4.8}$$

4.4. Concentration arithmetic mean normalization

Similarly, a normalization based on the arithmetic mean of donor and acceptor fluorophore concentrations can be defined. This is shown in equations (4.9) and (4.10)

$$\mathrm{arFRET}=\frac{2N_{\mathrm{D}}^{*}}{\left(N_{\mathrm{A}}+N_{\mathrm{A}}^{*}+N_{\mathrm{D}}+N_{\mathrm{D}}^{*}\right)}\,E, \tag{4.9}$$

$$\mathrm{arFRET}=\frac{2\mathrm{cFRET}}{\left(I^{\mathrm{AA}}\beta\mathrm{AER}\right)+\left(I^{\mathrm{DD}}\,\frac{\mathrm{DER}}{\alpha}+\mathrm{cFRET}\right)}. \tag{4.10}$$

The geometric mean of a set of numbers is always less than or equal to the arithmetic mean. Therefore, the

geometric normalization will always yield a higher FRET efficiency than the arithmetic normalization. The geometric and arithmetic normalizations will always give FRET efficiencies intermediate to the donor and acceptor normalizations.

4.5. Concentration ratio donors relative to acceptors

By combining equations (4.1), (4.2), (4.4) and (4.5), the ratio of the donor to acceptor concentration can be determined, as shown below

$$\frac{N_{\mathrm{D}}^{*}+N_{\mathrm{D}}}{N_{\mathrm{A}}^{*}+N_{\mathrm{A}}}=\frac{I^{\mathrm{DD}}\frac{\mathrm{DER}}{\alpha}+\mathrm{cFRET}}{I^{\mathrm{AA}}\beta\mathrm{AER}}. \tag{4.11}$$

4.6. Relative donor and acceptor concentrations

The donor and acceptor concentrations are used for normalization of the FRET signal to obtain the dFRET and aFRET measures. For time-lapse imaging, it is useful to be able to observe the relative changes in fluorophore concentration. The relative change in donor concentration between two measurements is given by

$$\frac{\left(I^{\mathrm{DD}}\frac{\mathrm{DER}}{\alpha}+\mathrm{cFRET}\right)_2}{\left(I^{\mathrm{DD}}\frac{\mathrm{DER}}{\alpha}+\mathrm{cFRET}\right)_1}, \tag{4.12}$$

and the relative change in acceptor concentration is given by

$$\frac{\left(I^{\mathrm{AA}}\right)_2}{\left(I^{\mathrm{AA}}\right)_1}. \tag{4.13}$$

4.7. Acceptor photobleaching

It is possible to quantify FRET using the acceptor photobleaching method. It is shown in appendix A that

$$\frac{N_{\mathrm{D}}^{*}}{N_{\mathrm{D}}^{*}+N_{\mathrm{D}}}E=\frac{1-\frac{I^{\mathrm{DD}}}{I_{\mathrm{AB}}^{\mathrm{DD}}}}{1-\frac{I^{\mathrm{DD}}}{I_{\mathrm{AB}}^{\mathrm{DD}}}(1-P_{\mathrm{B}})}, \tag{4.14}$$

where I^{DD} is the signal detected in the donor channel before photobleaching upon excitation at the donor wavelength and $I_{\mathrm{AB}}^{\mathrm{DD}}$ is the signal after photobleaching.

The method accounts for incomplete photobleaching with a factor P_{B}, representing the percentage of bleached photoacceptors. Thus, from equation (4.14) and by comparison with equation (4.1), one sees that the results obtained by photobleaching can be directly and quantitatively compared with those obtained using donor-normalized FRET in the sensitized emission method.

4.8. Interpretation of the various FRET normalizations in a biological context

In biological systems, the concentrations of fluorophores are often highly variable. For example, if the donor and acceptor fluorophores are tagged to two different proteins, then their distributions will vary with both the protein expression level and localization. That is why normalizing the obtained FRET signal for donor and acceptor concentrations is very important. It is also important that experiments from different laboratories with different experimental set-ups can be compared; a point that is hardly discussed in the current literature. For this reason, the various normalization methods described are defined so as to be independent of system parameters.

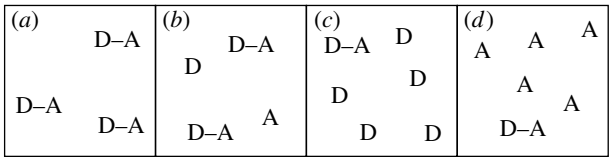

Figure 5. (*a–d*) Several donor–acceptor stoichiometries in which FRET may occur. See text for more details.

In FRET studies, the desired quantification is either the level of interaction between a single donor and a single acceptor (i.e. measuring E) or a measure of the fraction of donors and acceptors which interact (i.e. measuring $N_{\mathrm{D}}^{*}/(N_{\mathrm{D}}+N_{\mathrm{D}}^{*})$ or $N_{\mathrm{D}}^{*}/(N_{\mathrm{A}}+N_{\mathrm{A}}^{*})$), or simply the measurement of a positive FRET signal indicating that two proteins are interacting. In order to achieve these aims, it is critical to understand the various FRET signal normalizations outlined in the preceding sections. This is illustrated by considering several situations in more detail, as shown in figure 5.

First, consider the idealized case of equal donor and acceptor concentrations, where every donor interacts with one acceptor. This is illustrated in figure 5*a*. In this case, all normalizations presented earlier will yield the same value, and E can be determined. The fact that dFRET and aFRET are equal represents useful information—it shows that the total numbers of donors and acceptors are equal, i.e. one can define the stoichiometry of interaction to be 1 (see equation (4.11)).

Second, consider the case where the numbers of donor and acceptor fluorophores are equal, but not all are interacting (figure 5*b*). Again, all normalizations will yield the same result, but unless the fraction of interacting fluorophores is known, E cannot be determined. To determine E as well as the relative fractions of donors interacting would require additional methodologies, for example lifetime imaging with adequate resolution to permit the resolution of multiple lifetime components. Accurate fits to all time decay components do however require very large numbers of photons, which is not compatible with many biological experiments (Grailhe *et al.* 2006; Millington *et al.* 2007).

Next, consider the situation where there is an abundance of donor fluorophores, but donors and acceptors interact on a one-to-one basis (figure 5*c*). Here dFRET will be low, as there is a large free donor concentration. On the other hand, aFRET will be high, as all acceptors are interacting. Both geoFRET and arFRET will be intermediate in value. The best way to analyse this situation is to look at both donor and acceptor normalizations. This would then indicate that there is an interaction between the donor and acceptor, but that the donor was in a large excess. This information is not available when only geoFRET or arFRET are considered, as these quantifications represent a weighted average between the donor- and acceptor-normalized measurements. If only the donor-

normalized measurement is considered, then one might falsely conclude that no interaction is present as dFRET will be low. If acceptor photobleaching or mono-exponential donor lifetime imaging is used to analyse FRET in this situation, they would also indicate low FRET levels as they are equivalent to the donor normalization method.

Figure 5*d* shows the opposite case where the acceptor is in excess, but similar arguments still apply. Here analysis of geoFRET, arFRET, acceptor photobleaching or even multi-exponential donor lifetime imaging would not provide information on the excess of acceptor fluorophores, but analysis of aFRET and dFRET would.

For sensitized emission measurements, the best normalization strategy is to use both aFRET and dFRET and interpret them in combination. geoFRET and arFRET are not so useful as they are effectively just different weighted averages of aFRET and dFRET. By combining both aFRET and dFRET in any analysis, the maximum possible information content is extracted from sensitized emission measurements.

5. MATERIALS AND METHODS

5.1. Biological materials

5.1.1. Fluorophores. In the work presented here, enhanced CFP (ECFP), enhanced YFP (EYFP) (Rizzo *et al.* 2004) and cerulean (Cer), an improved form of CFP (Shaner *et al.* 2005), were used. Table 1 summarizes the spectral properties of these fluorophores.

5.1.2. Cell culture and transfection. All cell experiments reported were performed in HeLa cells. Cells were cultured in Dulbecco's modified Eagle's medium with sodium pyruvate, non-essential amino acids, supplemented with 10 per cent heat-inactivated foetal bovine serum, 1 per cent GlutaMAX-1 (200 mM), 1 per cent penicillin/streptomycin (10 000 U ml^{-1}) and 0.1 per cent fungizone (amphotericin B, 250 µg ml^{-1}) (all Invitrogen). Cells were cultured at 37°C and 10 per cent CO_2 and normally grown in 10 cm tissue culture Petri dishes (Nunc). For time-lapse imaging, cells were cultured on 0.17 mm glass bottom dishes (Willco Wells). For cell fixation experiments, cells were washed twice in PBS, and then incubated with 4 per cent paraformaldehyde (PFA) for 5–20 min at room temperature. HeLa cells were transfected using electroporation on an EquiBio electroporator operated at 1500 µF capacitance.

5.1.3. Plasmid construction and transformations. A positive FRET control construct was created by excising the EYFP gene from the pEYFP-N1 vector, and ligating it into the multiple cloning site of pECFP-C1 (both plasmids obtained from Clontech, Palo Alto, CA) by inserting a sequence coding for a short 18AA (amino acid) long polypeptide (GLRSRAQASNSAVEGSAM) between ECFP and EYFP. For the dynamic cell cycle, FRET imaging experiments of the cyclin–cdk complex cyclin B1, cyclin A and Cdk1 were labelled with FPs as follows: cyclin B1 and cyclin A were labelled with cerulean (Cer), a version of CFP with both quantum efficiency and extinction coefficients improved by approximately 50 per cent over ECFP (Shaner *et al.* 2005) and Cdk1 was labelled with EYFP. A negative FRET control was created by a single amino acid substitution at R202 (arginine to lysine) in cyclin B1 (from MRAIL to MKAIL in helix 1 of the cyclin box). This substitution resulted in cyclin B1 not being able to bind Cdk1 due to disruption of a necessary salt bridge, without significantly changing cyclin B1's overall structure (Kobayashi *et al.* 1992). DH5α bacteria (Invitrogen) were transformed using 200 ng DNA according to the manufacturer's instructions and DNA was isolated using Mini- and Maxi-prep kits (Qiagen).

Table 1. Spectral properties of ECFP, EYFP and Cer (Rizzo *et al.* 2004; Shaner *et al.* 2005). (EC, extinction coefficient; QY, quantum yield.)

fluorophore	Ex. peak (nm)	Em. peak (nm)	QY	EC ($M^{-1}\,cm^{-1}$)
ECFP	433	475	0.4	32 500
EYFP	514	527	0.61	83 400
Cer	433	475	0.62	43 000

5.2. Microscope platforms

Widefield FRET was performed on a Deltavision Spectris deconvolution microscope (Applied Precision, Seattle, WA) equipped with a 12 bit cooled CCD with 1.3 Mpixels (CoolSnap HQ v. 1.3, Roper Scientific). Illumination was provided by a 100 W mercury arc lamp. For time-lapse imaging, cells were maintained at optimum temperature and CO_2 levels using an environmental chamber (Solent Scientific). Details of relevance in the FRET analysis are listed in table 2.

Confocal CFP–YFP FRET imaging was performed on a Leica SP5 confocal laser scanning microscope. Details are listed in table 3.

In order to reduce artefacts due to sample movement, the microscope was operated in 'between line' mode, where for every image line, signals were first recorded with the donor excitation wavelength, immediately followed by excitation at the acceptor wavelength. For the same reason, signal averaging was performed using the 'line-averaging' feature on the microscope rather than 'frame averaging'.

For quantitative FRET imaging, it is essential that the photomultiplier detectors return a signal count that is linearly proportional to the number of photons emitted. The linearity of the detectors was measured for both excitation lines using the back reflection of a coverslip and operating the microscope in reflection mode.

Surprisingly, it was found that the microscope exhibited a severe nonlinearity at high signal count rates, which was verified in similar models owned by other researchers. In practice, linear operation was found to occur over less than 50 per cent of the full dynamic range in our system. We strongly advise performing such linearity checks, as detector nonlinearity hinders the possibility of achieving quantitative FRET applications.

Table 2. Parameters used for FRET imaging with the Deltavision microscope. (cw, centre wavelength in nm; bp, spectral bandpass in mm.)

property	value
donor excitation filter (nm)	436 cw/10 bp
acceptor excitation filter (nm)	500 cw/20 bp
donor emission filter (nm)	470 cw/30 bp
acceptor emission filter (nm)	535 cw/30 bp
objective	60× PlanAPO 1.4 NA oil immersion
CCD exposure time	200–3000 ms
data size	12 bit
zoom	1

Table 3. Parameters used for confocal FRET imaging on a Leica SP5 confocal microscope.

property	value
donor excitation wavelength	Ar:ion 458 nm line
acceptor excitation wavelength	Ar:ion 514 nm line
donor emission channel (nm)	470–494 nm
acceptor emission channel (nm)	530–545 nm
objective	63×1.4 NA oil immersion
scan speed	100 Hz
averaging	three-line average
PMT voltage	700–900 V
pinhole diameter	1–2 Airy units
data size	16 bit
zoom	1–4

Laser power fluctuations can cause errors in the AER measurement. Fluctuations were measured by recording the back reflection from a glass coverslip over a 30 min period, with the microscope operated in 'reflection' mode. Power fluctuations were significant over this time period (of the order 10%) but the fluctuations between the two lines were strongly correlated in time. It is the ratio of powers of the 458 and 514 nm line which influences errors in the AER amounting to ± 4 per cent. The axial overlap of the two beams was determined from axial intensity profiles obtained from z-image stacks. The peak of the profiles differed by less than 120 nm. This is considered insignificant in comparison with the full width at half-maximum of the z-profile, measuring approximately 1500 nm for a microscope pinhole of 2.0 Airy disc diameters. Image alignment errors between the different detection channels were below the optical resolution of our system.

5.2.1. TCSPC FLIM measurements. For the lifetime measurements, a modified Olympus FV300 confocal microscope was used, equipped with spectral detection capability and a TCSPC detection system (Becker and Hickl SPC 830). For excitation, a pulsed supercontinuum light source was used (Fianium SC450). Full details of the system are given in Frank *et al.* (2007). Images were analysed using the SPCImage software (Becker and Hickl).

6. RESULTS

6.1. Calculation of α and β

The FRET software developed here enables calculation of α (equation (4.3)) and β (equation (4.6)) from the transmission spectra of emission and excitation filters, fluorophore spectral characteristics, etc. Spectral information can be entered and overlap factors and transmission efficiencies are automatically calculated. It should be noted, however, that published data on fluorophore spectra and quantum yields may not be representative of corresponding properties in actual experimental samples under investigation. Changes in pH, local environment, molecular association and conformation, changes in refractive index, etc. all affect a fluorophore's spectral properties (Lakowicz 1999).

If accurate spectral data on fluorophores and detection systems are not available, we propose the use of a positive FRET control construct for which the transfer efficiency E has been determined independently, e.g. by lifetime imaging (preferred method) or by the acceptor photobleaching method. The data are compared with the results of the sensitized emission approach (i.e. comparisons of equations (2.4), (4.2), (4.5) and (4.14)). For all data reported here, the 18AA linker construct was used as described in §5.1. A calibration construct thus characterized can then be used directly for FRET analysis and serves as a standard that is transferable from instrument to instrument.

Table 4 lists the results obtained for the different cell types, fluorophores, and microscopy systems used. There are notable differences between the live cell and PFA fixed cells obtained under the same measurement conditions, representative of the effect of fixation on the fluorophore spectral properties. Cer has similar excitation and emission spectra to ECFP but a much larger quantum yield (table 1) and these cause differences of α and β between Cer–EYFP and ECFP–EYFP.

6.2. Validation of protocols with FRET control constructs

The 18AA tandem constructs were used to validate whether the sensitized emission normalization methods could quantify the effect of the addition of extra free donors or extra free acceptors (i.e. a change in the stoichiometry of the interaction). As a negative control, ECFP and EYFP were co-expressed in cells. Any FRET signal in this system would indicate that intracellular concentrations of the fluorophores were too high, hence giving rise to FRET by molecular proximity and crowding (Grailhe *et al.* 2006). Finally, samples with only ECFP and only EYFP were prepared in order to measure the DER and AER, respectively. In order to check the sensitized emission measurements, and for the calibration of the α and β factors, samples were also tested using the acceptor photobleaching method and TCSPC.

Estimates of the errors for measurements in cells are presented in two ways. The error within an individual cell was estimated in terms of the average standard

Table 4. Summary of the α and β values determined from positive control constructs.

fluorophores	microscope	D Ex. (nm)	A Em. (nm)	α	β
ECFP+EYFP	confocal	458	530–545	0.19	2.5
ECFP+EYFP	confocal (fixed)	458	530–545	0.22	3.4
ECFP+EYFP	widefield	436	520–550	0.22	18
Cer+EYFP	widefield	436	520–550	0.34	23

Table 5. Lifetimes measured by TCSPC for the 18AA constructs and free ECFP in live and fixed cells. (ECFP in both live and fixed cells shows a similar lifetime. In the 18AA constructs, the lifetime is reduced due to the presence of FRET.)

sample	mean τ (ps)	mean σ in a cell (ps)	σ_E in mean (ps)	95% CI for mean (ps)
18AA	1549	124	15	30
ECFP	2513	124	13	26
18AA fixed	1976	123	15	30
ECFP fixed	2514	200	9	18

deviation of pixels within a cell. The error in the mean value from all cells was estimated by calculating a 95% confidence interval based on the standard error in the mean values.

6.2.1. TCSPC results. TCSPC measurements were used to estimate the transfer efficiency of 18AA constructs in both live and fixed cell environments. ECFP-only samples in the same conditions were used to measure the lifetime of the donor in the absence of FRET.

To determine the number of exponentials required to obtain a good fit, the data from all pixels in an image were spatially binned in order to create a 'super pixel'. This super pixel had a large number of photons (over a million) and so all exponential components contributing to the decay curve could be resolved. Increasing numbers of exponentials were fitted until no improvement in the reduced chi-squared value or structure of the residuals was seen. For the 18AA constructs, it was found that three exponentials gave the best fit. For the ECFP samples, it was found that two exponentials gave the best fit. This is in good agreement with the previous findings (Duncan *et al.* 2004; Millington *et al.* 2007). On a pixel-by-pixel basis, the signal-to-noise ratio was too low to fit three exponential components reliably. Under these conditions, the mean lifetime obtained by the fit is the most reliable quantity to use and this was used to calculate the transfer efficiency, as shown in equation (2.4). Hence the transfer efficiency calculated was a mean transfer efficiency, which can be compared with the one calculated from sensitized emission or acceptor photobleaching measurements.

The results of the lifetime imaging are shown in table 5. Sample images from the data are shown in figure 6. The mean transfer efficiency, as calculated from equation (2.4), is shown in table 6.

The results from the TCSPC imaging show that the 18AA constructs have a different mean transfer efficiency in live compared with fixed cells. These observations are indicative of the different molecular matrix the fluorophores are embedded, in living cells

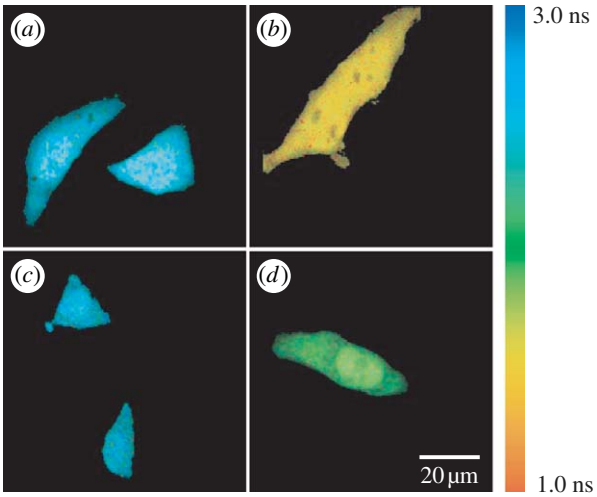

Figure 6. Sample TCSPC images: (*a*) ECFP only in live cells, (*b*) 18AA constructs in live cells, (*c*) ECFP only in fixed cells and (*d*) 18AA constructs in fixed cells. All images are intensity-lifetime overlay images exported from SPCImage. The results of the TCSPC data are summarized in table 5.

Table 6. Mean transfer efficiencies E measured by TCSPC for the18AA constructs in live and fixed cells. (The live cell samples show a higher level of FRET than the fixed samples.)

sample	mean E (%)	95% CI for mean (%)
18AA	38.4	1.9
18AA fixed	21.4	1.8

compared with fixed cells, where there are increased levels of molecular cross-linking. Changes in the shape of fluorophore excitation or emission spectra, donor quantum yield, orientation factor (κ^2) or medium refractive index all directly influence the Förster radius.

6.2.2. Acceptor photobleaching results. The acceptor photobleaching technique was applied both on widefield and confocal systems using the Deltavision and Leica

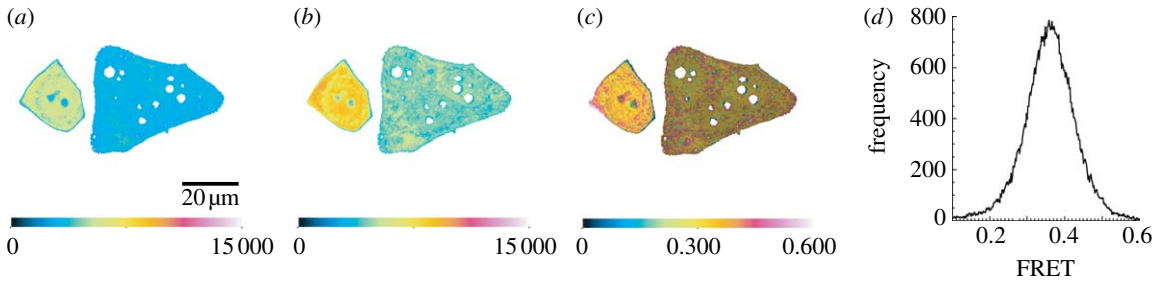

Figure 7. Sample image demonstrating the acceptor photobleaching method on the Leica SP5 confocal microscope: (*a*) I^{DD} image before bleaching, (*b*) I^{DD} image after bleaching, (*c*) false colour intensity-overlay FRET image and (*d*) histogram showing the FRET distribution.

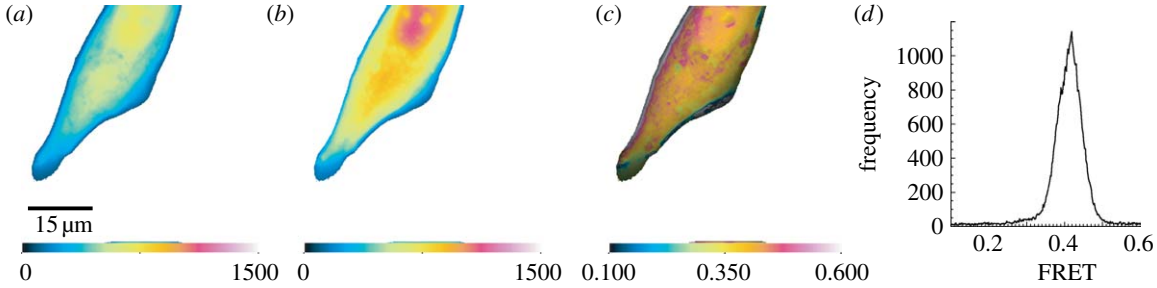

Figure 8. Sample image demonstrating the acceptor photobleaching method on the Deltavision widefield microscope: (*a*) I^{DD} image before bleaching, (*b*) I^{DD} image after bleaching, (*c*) false colour intensity-overlay FRET image and (*d*) histogram showing the FRET distribution.

SP5 microscopes, respectively. The results obtained matched closely for both methods and were also in good agreement with the TCSPC results. Example images are shown in figures 7 and 8 from the confocal and widefield microscopes, respectively. The results are summarized in table 7. Here I^{DD} refers to the image acquired in the donor emission channel upon excitation with the donor excitation wavelength. Similarly I^{DA} and I^{AA} refer to the image acquired in the acceptor emission channel upon excitation with the donor and acceptor excitation wavelengths, respectively.

Some artefacts can be seen in the photobleaching images due to cell movement in the time between the before- and after-bleaching images were recorded. This increases the standard deviation of FRET levels within a cell.

6.2.3. Sensitized emission results. Using the developed sensitized emission software, images from both the Deltavision and Leica SP5 microscopes were analysed and compared. A sample set of typical results is shown in figures 9 and 10. Table 8 summarizes all of the sensitized emission results.

For the tandem construct imaging, the results of the TCSPC and acceptor photobleaching measurements match very well. They also agree with the sensitized acceptor emission measurements, since the α and β values were chosen based on the TCSPC results (figure 11). Even though the widefield and confocal measurements were performed on entirely different systems, the sensitized emission FRET measurements still match. This highlights one of the benefits of the developed analysis technique, as it allows comparison of measurements from different laboratories, which was not possible with some of the previously reported sensitized emission FRET quantification methods.

Table 7. Photobleaching transfer efficiencies for 18AA constructs measured on the Deltavision and Leica SP5 microscopes.

sample	mean E (%)	95% CI for mean (%)	mean σ in E in a cell (%)
18AA Deltavision	37.6	3.9	8.0
18AA Leica SP5	35.2	1.2	8.4

When extra CFP was co-transfected as well as 18AA constructs, there was a marked decrease in dFRET, while aFRET remained at the level expected for 18AA constructs. The analogous case for extra YFP was also true. This was exactly as predicted by the theoretical analysis, and demonstrates the improved level of quantification that is achievable if both donor and acceptor normalization strategies are used.

The results also show that the samples which were co-transfected with non-linked CFP and YFP exhibit FRET levels which are not significantly different from zero. This demonstrates the usefulness of such samples as a negative control. It also shows that, for the cells investigated, CFP and YFP concentrations were not high enough to cause appreciable FRET to occur due to molecular proximity. At higher concentrations, this may of course change.

In combination, the use of the 18AA constructs and CFP–YFP co-transfection samples aids a great deal in the quantification of sensitized emission FRET measurements. They provide negative as well as

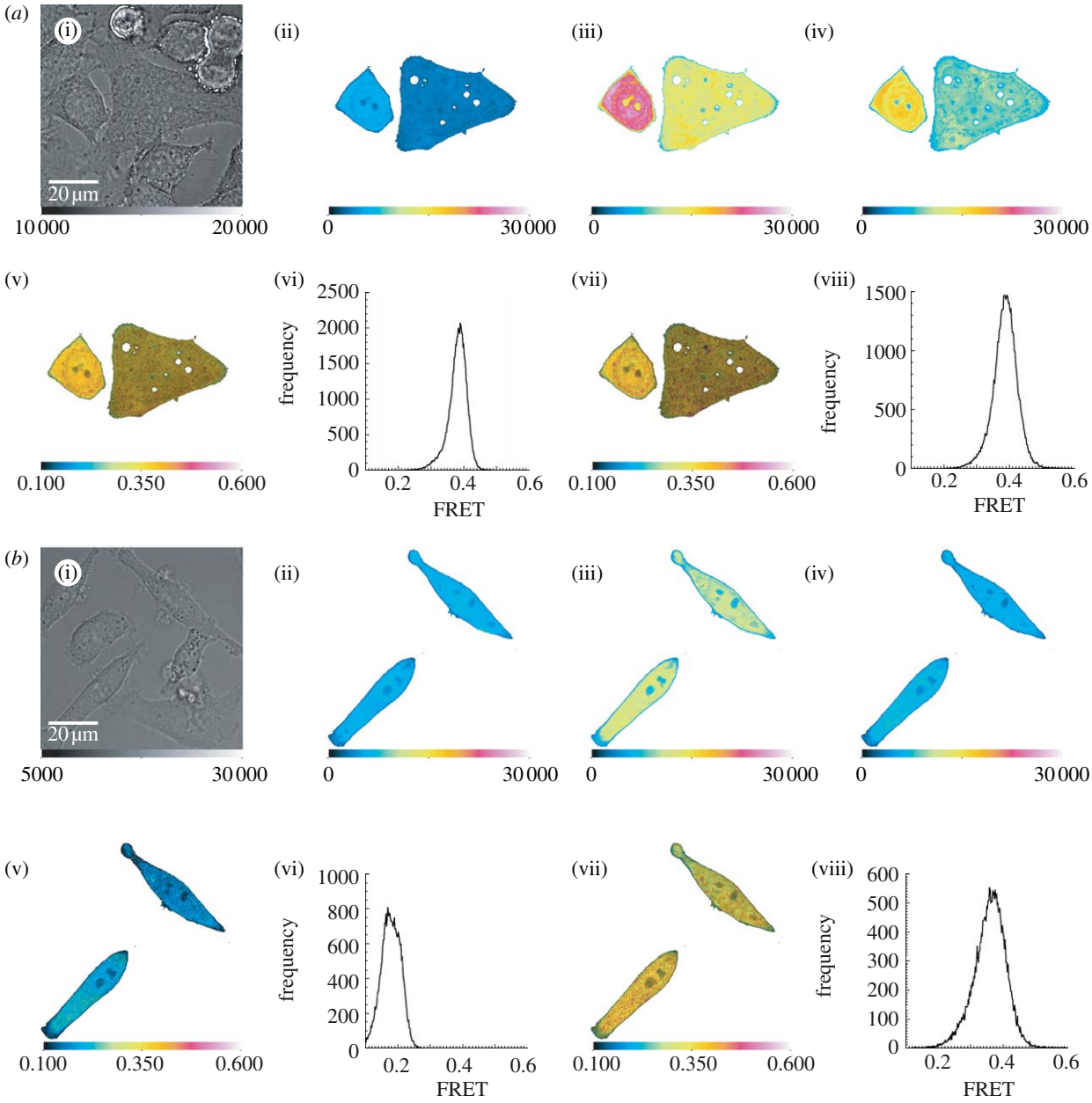

Figure 9. Sample data using the Leica SP5 confocal microscope. (*a*) Data for 18AA FRET construct. (i) Transmission image, (ii) I^{DD}, (iii) I^{DA}, (iv) I^{AA}, (v and vi) dFRET and (vii and viii) aFRET. (*b*) Sample data for 18AA FRET constructs with additional CFP. (i) Transmission image, (ii) I^{DD}, (iii) I^{DA}, (iv) I^{AA}, (v and vi) dFRET and (vii and viii) aFRET.

positive controls, and permit a rigorous normalization to obtain concentration-weighted transfer efficiencies by providing the experimenter with an easy method for the determination of the α and β values. Measurements analysed in this manner provide values of the transfer efficiency, which are independent of the hardware platform used for the measurement.

6.3. Investigation of dynamic protein–protein interactions

The developed technique was used for dynamic imaging of interactions in the cyclin–cdk family of proteins in living cells. Cdks play a key role in the regulation of mitosis (Morgan 2007). Cdks are serine–threonine kinases whose substrate binding site is obscured by the so-called T-loop structure. When cyclins bind to cdks, the T-loop is relocated and the cdk becomes activated to permit substrate binding (Russo *et al.* 1996). In the work presented here, we follow the assembly and destruction of cyclin–cdk complexes in real time. Interactions were measured between cyclin B1 and cdk1 and cyclin A and cdk1. Use of the sensitized emission FRET analysis enabled time-lapse imaging throughout the cell to be performed and changes in the bound and unbound fractions to be visualized in a dynamic fashion.

For the cyclin B1 and cdk1 studies, cyclin B1 was tagged with cerulean and cdk1 with EYFP. The sensitized emission analysis showed a dFRET signal of approximately 8 per cent compared with an aFRET level of 2 per cent, indicating that the two proteins were

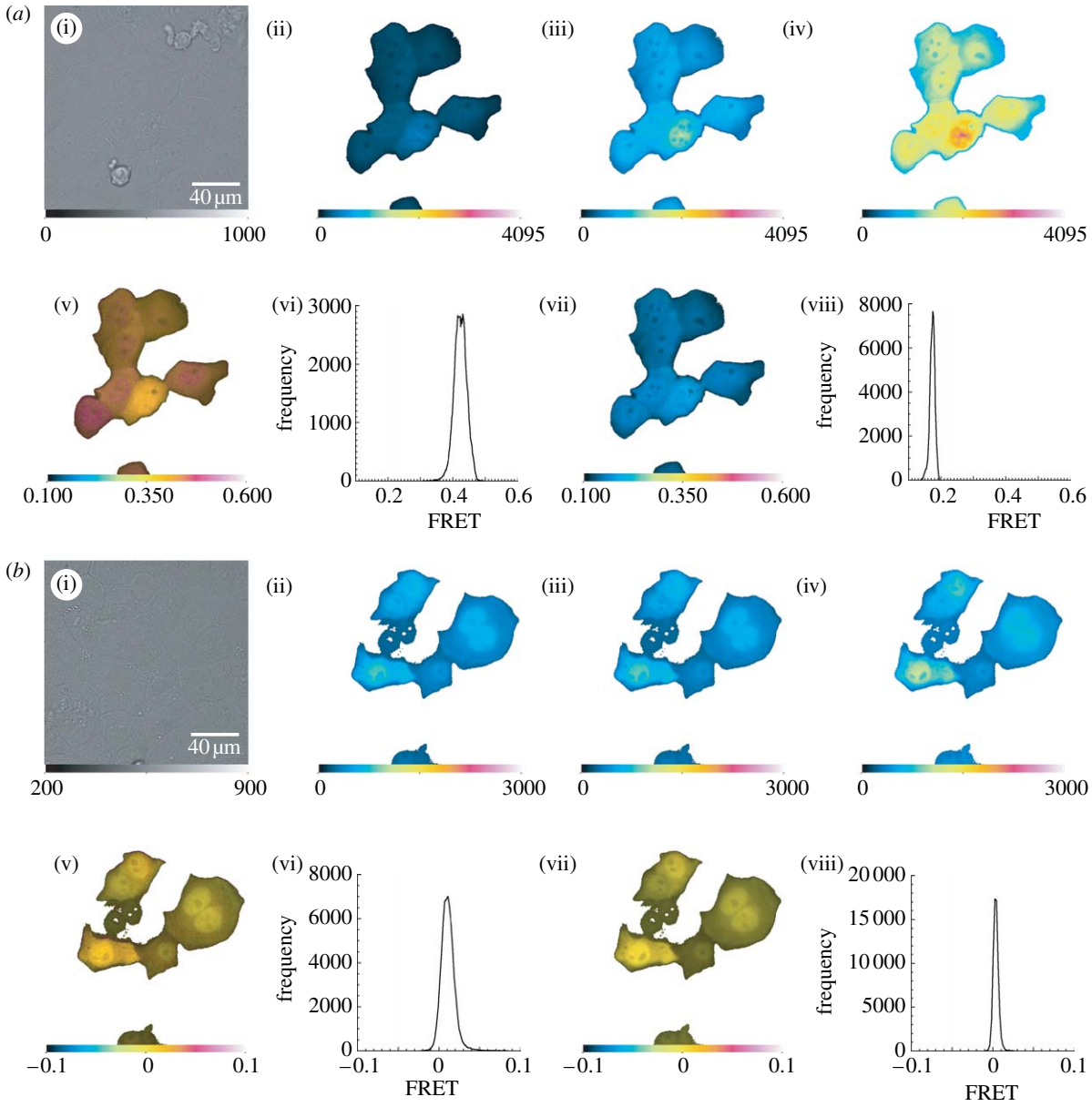

Figure 10. Sample data using the Deltavision microscope. (*a*) Data for 18AA FRET construct with additional YFP. (i) Transmission image, (ii) I^{DD}, (iii) I^{DA}, (iv) I^{AA}, (v and vi) dFRET, (vii and viii) aFRET. (*b*) Sample data for cells co-transfected with CFP and YFP. (i) Transmission image, (ii) I^{DD}, (iii) I^{DA}, (iv) I^{AA}, (v and vi) dFRET, (vii and viii) aFRET.

Table 8. Measured sensitized emission transfer efficiencies on the Leica SP5 and Deltavision for 18AA constructs, and 18AA constructs with additional CFP or YFP and CFP + YFP. (CIs based on $N=2\pm5$ cells.)

	18AA	18AA+CFP	18AA+YFP	CFP+YFP
Leica SP5				
dFRET	36.9	18.3	38.7	−0.1
aFRET	36.8	36.8	28.4	−0.5
95% CI for dFRET mean	1.4	1.5	1.6	0.5
95% CI for aFRET mean	1.4	1.2	1.9	0.7
mean σ_{dFRET} in a cell	2.8	2.8	3.1	2.5
mean σ_{dFRET} in a cell	3.4	5.2	2.8	3.7
Deltavision				
dFRET	38.7	20.3	44.0	2.6
aFRET	36.6	36.7	1.4	0.9
95% CI for dFRET mean	1.2	1.0	1.2	0.6
95% CI for aFRET mean	0.7	0.8	1.1	0.2
mean σ_{dFRET} in a cell	1.1	1.5	1.0	1.0
mean σ_{dFRET} in a cell	0.8	1.6	0.7	0.3

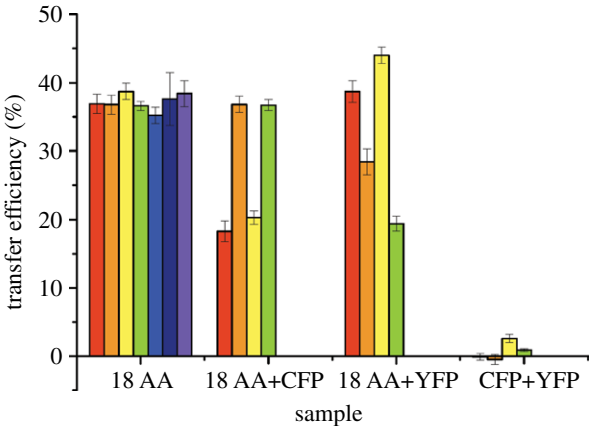

Figure 11. Comparison of all tandem construct data. The error bars represent 95% confidence intervals for the mean of all samples imaged ($N=2\pm5$ cells). Red, Leica dFRET; orange, Leica aFRET; yellow, DV dFRET; green, DV aFRET; blue, Leica P Bleach; indigo, DV P Bleach; purple, TCSPC.

interacting. The difference between dFRET and aFRET signifies varying fluorophore concentrations. In this case, the acceptor fluorophore concentration is high, causing the acceptor normalization to be lower. Figure 12 shows a sample image from this experiment.

As a control, the experiment was repeated with a single amino acid substitution at R202 (arginine to lysine) in cyclin B1, from MRAIL to MKAIL in helix 1 of the cyclin box, which is known to prevent cyclin B1–cdk1 binding (Kobayashi *et al.* 1992). Despite the fact that MKAIL B1 and CDK still colocalized strongly in the cells, no significant FRET signal was detected (table 9). This secondary experiment provides a biological negative control for the verification of the protein–protein interaction. It proves that the sensitized emission analysis is effective for verifying protein–protein interactions, and that the observed signals are not due to colocalization and FP dimerization. A sample image from the cyclin B1 MKAIL–cdk1 experiment is shown in figure 13.

The second system investigated was that of cyclin A and cdk1, tagged with cerulean and EYFP, respectively. Initially, the system was investigated measuring FRET in single images, and then progressed to time-lapse imaging to monitor FRET throughout the cell cycle. The results of the FRET analysis for single images indicated that the two proteins were interacting, as can be seen in the example image (figure 14) and the mean data from all cells analysed (table 10).

The time-lapse imaging showed not only that the proteins were interacting, but also that the levels of interaction changed during the course of the cell cycle. Figure 15 shows the raw data and FRET analysis for a few example frames taken from a sample time-lapse series. Figures 16 and 17 show how the FRET and protein concentration levels vary with time for two example cells. Movies of these interactions are found in the electronic supplementary material.

Examining all the measured signals, as in the data presented in figures 16 and 17, allows for a more complete analysis of what the changing FRET signals mean. In particular, looking at the relative changes in the signals with time can give insight into the processes occurring.

When the cell enters mitosis, cyclin A starts to be degraded, as indicated by the decreasing donor concentration. Cdk1 concentrations, however, tend to keep rising (note that the rise of ectopic cdk1 may be affected somewhat by residual translation and maturation of FPs). Initially dFRET rises and aFRET stays approximately constant, but rising slightly (region 1). Then, after a certain point, both dFRET and aFRET decrease until eventually the fluorescence signal becomes too low for analysis (region 2). Shortly afterwards, the cell divides. The changing FRET signals can be matched to points in the cell cycle but here the emphasis is placed on the physical interpretation rather than the particular biological implications.

In region 1, dFRET rises. Assuming that the actual FRET efficiency of a single donor–acceptor interaction does not change, then with reference to equation (4.1), this means that the ratio of interacting to total donor fluorophores increases. Since the total donor fluorophore concentration is decreasing, this means that the non-interacting donor concentration is decreasing faster than the interacting donor concentration. In fact, when the cFRET signal is examined, it is seen that the number of interacting donors is actually increasing in region 1. aFRET stays approximately constant (with only a slight rise) because the increasing number of interacting acceptor fluorophores is offset by the increasing total acceptor fluorescence. In region 2, both aFRET and dFRET fall, as does the donor fluorophore concentration. The acceptor fluorophore concentration, however, rises. The falling dFRET signal means that the number of interacting fluorophores falls faster than the total number of donor fluorophores.

To summarize, it is seen that there are two clearly identifiable regions of behaviour. The first where free donor is degraded, but interacting donor increases, and the second where both free donor and interacting donor levels fall, with the interacting donor levels falling at a faster rate. The interacting donor levels could fall because of two reasons: either the protein–protein complex falls apart or interacting donor is degraded. Either way, the analysis clearly identifies a point at which the interaction between the two proteins starts to cease.

To ensure that the observed decrease in FRET was not due to effects caused by imaging the cells for an extended time period, cells that did not enter mitosis were also analysed. This is demonstrated in figure 18. Here the cell does not enter mitosis, and the FRET levels remain approximately constant throughout the imaging period. The patterns observed in figures 16 and 17 for cells proceeding normally through mitosis and in figure 18 for non-dividing cells were reproducibly observed for all cells analysed ($N=20\pm5$).

This analysis clearly demonstrates one of the great advantages of the sensitized emission technique; because the technique is fast and non-destructive, it can be used to monitor the change in FRET with time from many different cells in a sample dish with a high time resolution (order of minutes) and over long periods (order of hours). As an example, collecting all the necessary images for a typical experiment on the

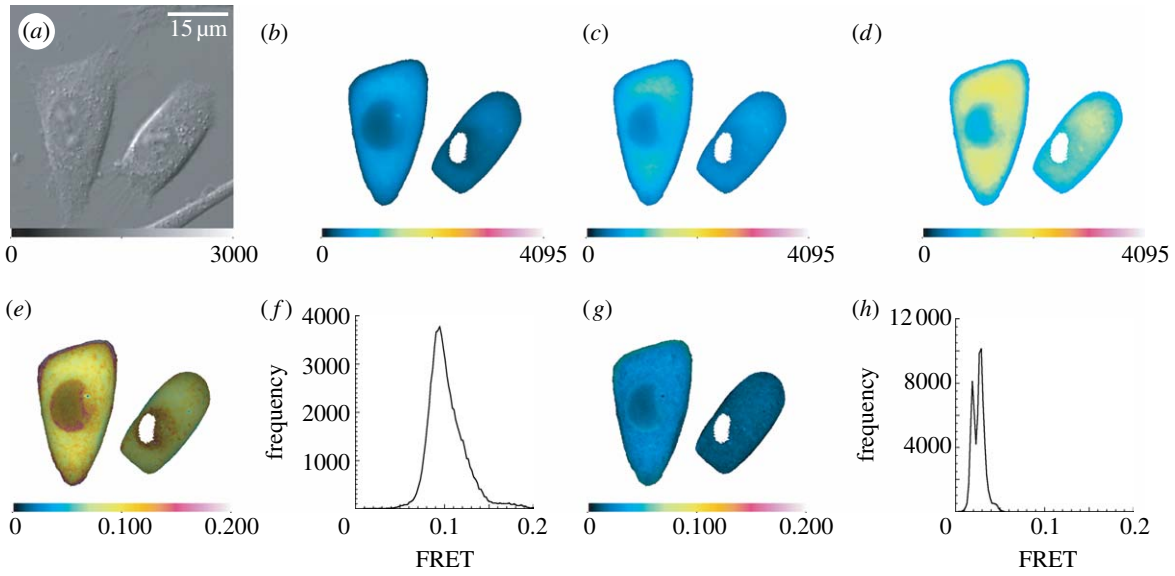

Figure 12. Intensity images and sensitized emission FRET analysis data for cyclin B1 tagged with cerulean and cdk1 tagged with YFP. (*a*) Transmission image, (*b*) I^{DD} image, (*c*) I^{DA} image, (*d*) I^{AA} image, (*e*) dFRET image, (*f*) dFRET histogram, (*g*) aFRET image, (*h*) aFRET histogram.

Table 9. Measured transfer efficiencies for cyclin B1–cerulean and cdk1–EYFP with and without the MKAIL mutation ($N=2\pm5$ cells).

	dFRET	mean σ_{dFRET}	95% CI for dFRET	aFRET	mean σ_{dFRET}	95% CI for aFRET
MRAIL	8.4	1.9	1.2	2.0	0.5	0.4
MKAIL	0.9	1.6	0.9	0.2	0.4	0.2

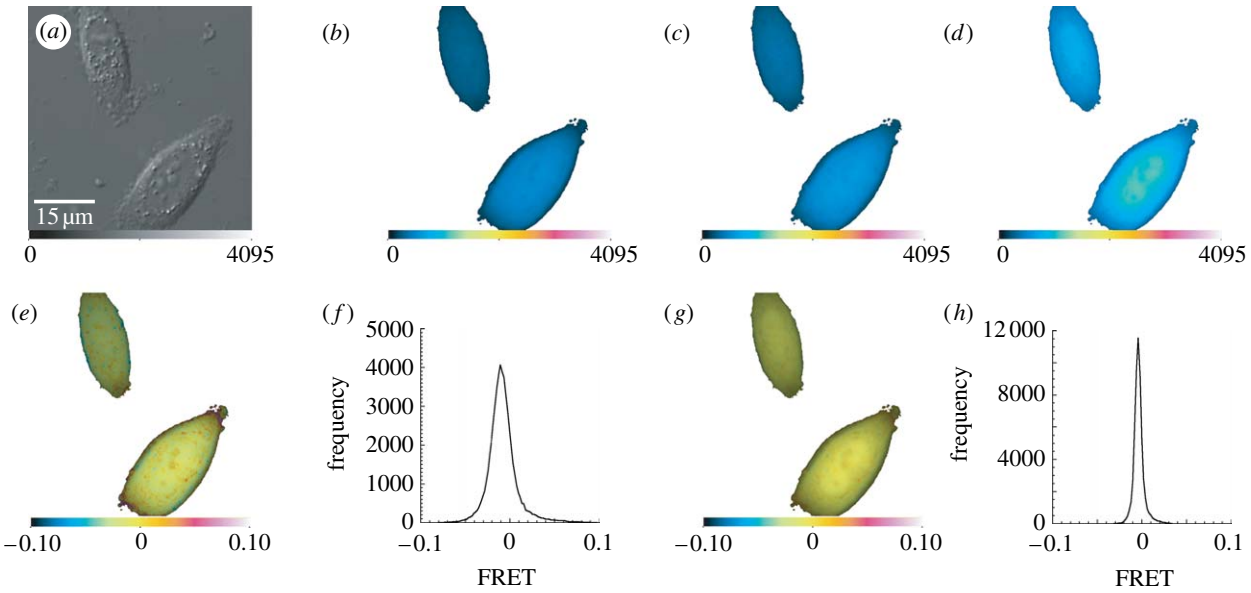

Figure 13. Intensity images and sensitized emission FRET analysis data for cyclin B1 with the MKAIL mutation tagged with cerulean and cdk1 tagged with YFP. (*a*) Transmission image, (*b*) I^{DD} image, (*c*) I^{DA} image, (*d*) I^{AA} image, (*e*) dFRET image, (*f*) dFRET histogram, (*g*) aFRET image, (*h*) aFRET histogram.

Deltavision microscope takes approximately 3 s. This allows many different cells to be imaged within a 2 min cycle, using the Deltavision's sample positioning system. Samples can be imaged for hundreds of cycles to collect the required data—cells have been successfully imaged for over 6 hours continuously.

7. CONCLUSIONS

Measurement of FRET by sensitized emission has several key advantages—it requires minimal hardware to implement and is widely applicable across different platforms. Its most potent advantages are the facts that it is a non-destructive method that is

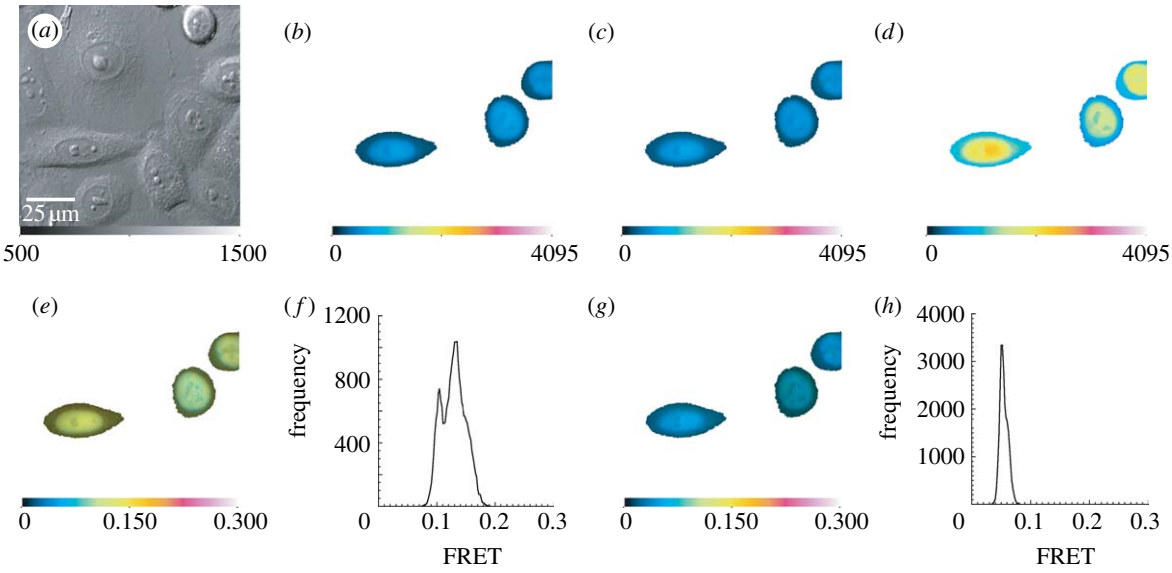

Figure 14. Intensity images and sensitized emission FRET analysis data for cyclin A tagged with cerulean and cdk1 tagged with EYFP. (*a*) Transmission image, (*b*) I^{DD} image, (*c*) I^{DA} image, (*d*) I^{AA} image, (*e*) intensity-overlay dFRET image, (*f*) dFRET histogram, (*g*) intensity-overlay aFRET image, (*h*) aFRET histogram.

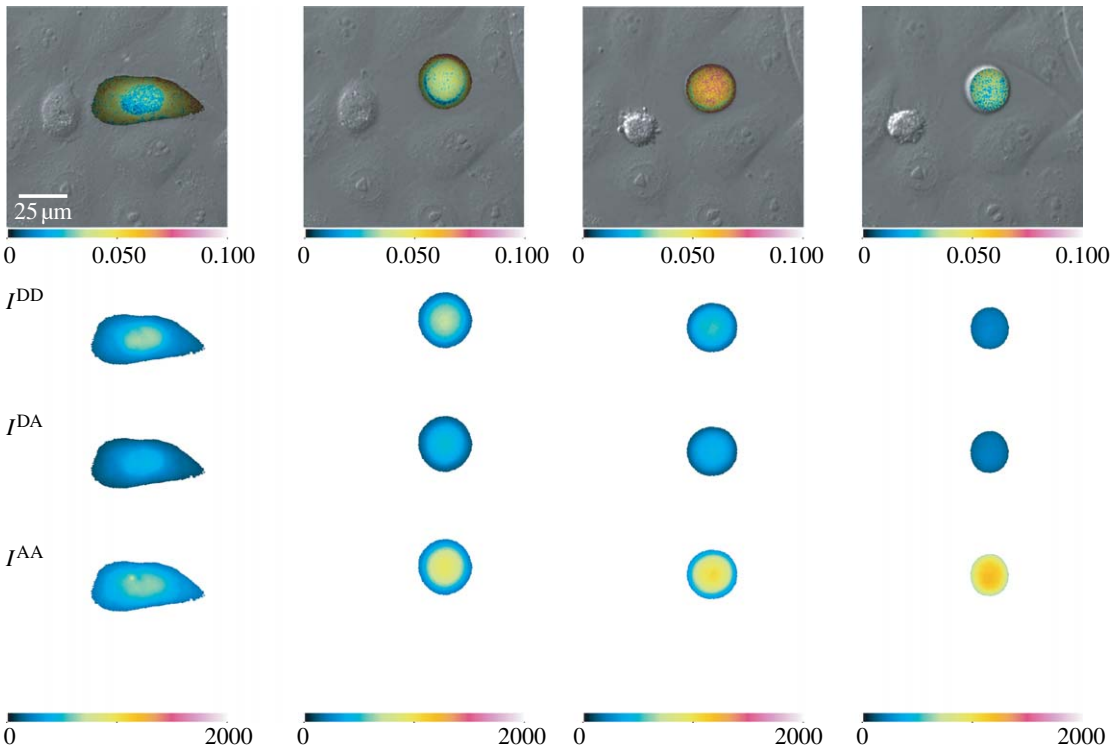

Figure 15. Intensity images (trans-dFRET) and sensitized emission FRET analysis data for cyclin A tagged with cerulean and cdk1 tagged with EYFP for a time-lapse series of measurements. Data are shown from time points at 0, 44, 125 and 278 min. Full movies are available in the electronic supplementary material.

Table 10. Measured transfer efficiencies for cyclin A–cerulean and cdk1–EYFP ($N=2\pm5$ cells).

	dFRET	mean σ_{dFRET}	95% CI for dFRET	aFRET	mean σ_{dFRET}	95% CI for aFRET
cyclin A–cdk1	9.8	1.2	1.5	5.5	0.6	0.2

sensitive enough to permit imaging at high speed and over extended periods of time, making it the method of choice for the verification of dynamic molecular interactions in living cells.

A key problem with FRET-sensitized fluorescence methods lies in the quantification of obtained signals. The first problem arises from crosstalk: both donor emission bleed-through and acceptor cross-excitation

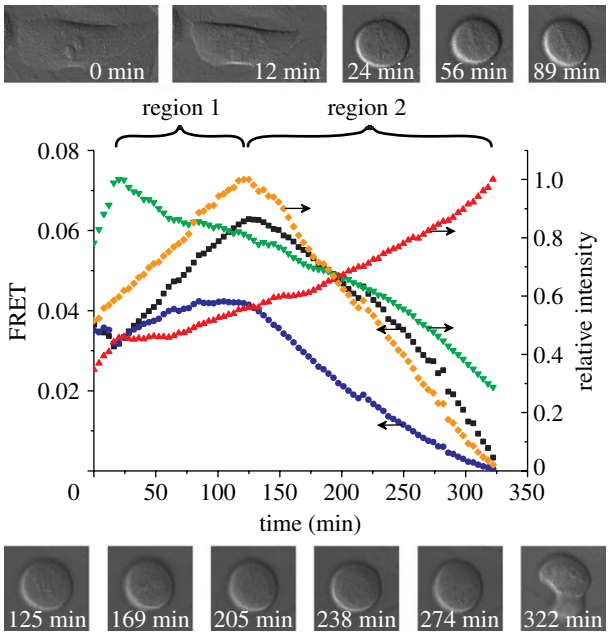

Figure 16. Sample image showing the variation in FRET and protein concentration with time for cyclin A–cerulean and cdk1–EYFP. Transmission images at different times are inlaid to indicate the cell's procession through mitosis. Squares, dFRET; circles, aFRET; downtraingles, donor concentration; uptriangles, acceptor concentration; diamonds, cFRET.

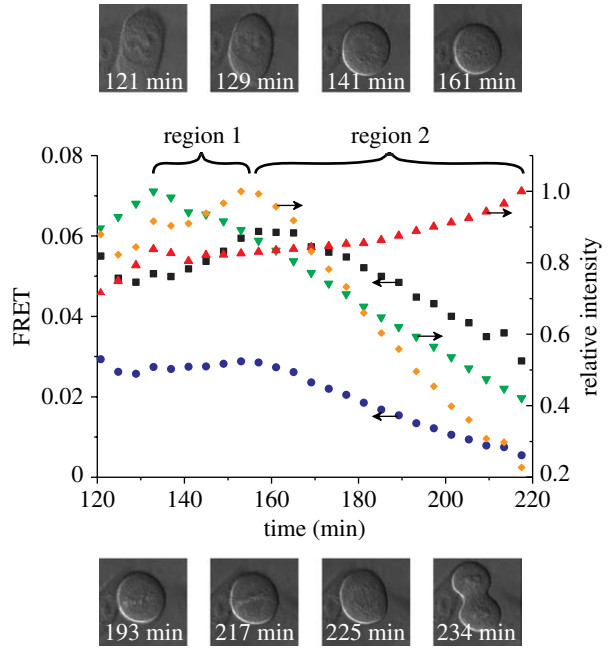

Figure 17. Second sample image showing the variation in FRET and protein concentration with time for cyclin A–cerulean and cdk1–EYFP. Transmission images at different times are inlaid to indicate the cell's procession through mitosis. Squares, dFRET; circles, aFRET; downtraingles, donor concentration; uptriangles, acceptor concentration; diamonds, cFRET.

contaminate the sensitized emission signal. The literature abounds with corrections for these factors, which can become confusing to the potential user, even though all the published algorithms are essentially the same. The second, and more difficult issue to consider, is the normalization of the measured FRET signal for fluorophore concentration and imaging system parameters, so that experiments obtained in different environments and with different fluorophore systems can be directly compared. Signal normalization is extremely important, to the point where it may be the deciding factor in establishing whether FRET occurs or not, yet it is not properly considered in many publications presenting FRET data.

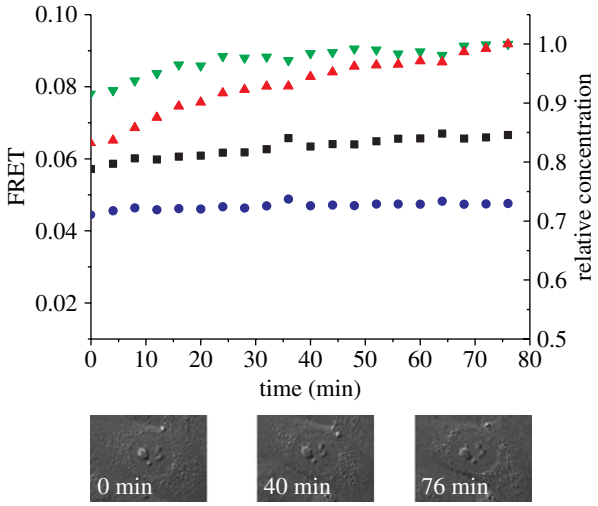

Figure 18. Sample image showing the variation in FRET and protein concentration with time for cyclin A–cerulean and Cdk1–EYFP in a cell that did not enter mitosis. Transmission images at different times are inlaid to indicate that the cell does not enter mitosis. Squares, dFRET; circles, aFRET; downtriangles, donor concentration; uptriangles, acceptor concentration.

Here we provide a rigorous theoretical framework for FRET analysis by sensitized emission using a model of FRET, which is both intuitive to understand and practical to apply in an experimental context. Optimal normalization strategies were considered and validated with live cell samples, and it is shown that the combined use of two measures of FRET-sensitized emission, namely dFRET and aFRET (for donor- and acceptor-normalized FRET) offer a maximum of information from an experiment. The combined use of aFRET and dFRET was shown to provide information both on fractions of interacting fluorophores and on the strength of FRET interaction. The model has been implemented in a freely available, user-friendly analysis software that operates on a variety of computer platforms.

Verification of the technique was performed on both confocal and widefield systems by imaging linked ECFP–EYFP constructs exhibiting known levels of FRET, along with comparison of the results with donor lifetime-imaging and acceptor photobleaching measurements. The capability of the method to provide data on the interaction stoichiometry was validated using a positive CFP–YFP control construct, for which the stoichiometry of interaction was 1. Introducing a deliberate change of interaction stoichiometry by coexpression of surplus (free) donor and acceptor fluorophores showed conclusively that the method can quantify these stoichiometric changes.

We applied the developed protocols for the investigation of protein–protein interactions in living cells. In addition to the usual negative controls for sensitized emission FRET experiments, we show the importance of using a positive, FRET exhibiting control construct to confirm whether proteins interact by FRET or not. Finally, we apply the protocol for real-time imaging of interactions between the cyclin–cdk family of proteins in living cells and follow these interactions through mitosis. FRET levels between the CER- and EYFP-tagged proteins were monitored as the cells progressed through mitosis. Examining how the FRET normalizations and fluorophore concentrations changed throughout a time-lapse experiment enabled conclusions to be drawn on the relative changes in the stoichiometry of the interaction (i.e. the relative amounts of free to interacting protein).

We would like to thank Dr Uwe Rauch from the Medical Faculty at the University of Lund, Sweden, for invaluable advice and initial preparation of the linked FRET control constructs.

APPENDIX A

A.1. Derivation of dFRET

The fluorescence intensity of a system upon excitation with intensity I_{ex} is given by

$$I = \left(\frac{BI_{\mathrm{ex}}\Gamma}{c}\right) NQ\psi, \tag{A 1}$$

where the first term in brackets corresponds to the rate of excitation of the fluorophore; N is the number of fluorophores in the ground state; Q is the fluorescence quantum yield; and ψ is the collection efficiency of the detection channel; B is the Einstein coefficient for stimulated absorption; I_{ex} is the excitation spectral irradiance assumed to be below saturation levels for the transition probed; c is the speed of light; and Γ is the spectral overlap factor between the excitation light and the absorption spectrum of the fluorophore.

In a sample with donors and acceptors, the total number of donors is given by $N_{\mathrm{D}} + N^*_{\mathrm{D}}$, where N_{D} is the number of donors that are outside interaction distance, and N^*_{D} is the number of donors within FRET interaction distance. The amount of donor signal $I^{\mathrm{DA}}_{\mathrm{D,\,noFRET}}$ detected in the acceptor channel, had no FRET occurred, is given by

$$I^{\mathrm{DA}}_{\mathrm{D,\,noFRET}} = \left(\frac{B^{\mathrm{D}}_{\mathrm{D}} I_{\mathrm{ex,D}} \Gamma^{\mathrm{D}}_{\mathrm{D}}}{c}\right)(N_{\mathrm{D}} + N^*_{\mathrm{D}})\, Q_{\mathrm{D}}\psi^{\mathrm{A}}_{\mathrm{D}}. \tag{A 2}$$

On the other hand, the true amount of FRET signal cFRET, which is free of crosstalk, is given by

$$\mathrm{cFRET} = \left(\frac{B^{\mathrm{D}}_{\mathrm{D}} I_{\mathrm{ex,D}} \Gamma^{\mathrm{D}}_{\mathrm{D}}}{c}\right) Q_{\mathrm{A}}\psi^{\mathrm{A}}_{\mathrm{A}} N^*_{\mathrm{D}} E, \tag{A 3}$$

where $N^*_{\mathrm{D}}E$ is the actual number of donor molecules within interaction distance, which transfer energy to the acceptors. Dividing equation (A 3) with (A 2) and comparing the result with equation (4.1), we obtain

$$\mathrm{dFRET} = \frac{\mathrm{cFRET}}{I^{\mathrm{DA}}_{\mathrm{D,\,noFRET}}}\,\alpha, \tag{A 4}$$

where

$$\alpha = \frac{Q_{\mathrm{D}}\psi^{\mathrm{A}}_{\mathrm{D}}}{Q_{\mathrm{A}}\psi^{\mathrm{A}}_{\mathrm{A}}}. \tag{A 5}$$

Now the total number of donor molecules can be written as

$$N_{\mathrm{D}} + N^*_{\mathrm{D}} = ((1-E)N^*_{\mathrm{D}} + N_{\mathrm{D}}) + N^*_{\mathrm{D}}E. \tag{A 6}$$

Here $(1-E)N^*_{\mathrm{D}} + N_{\mathrm{D}}$ is the number of non-interacting donor molecules and $N^*_{\mathrm{D}}E$ is the number of interacting donor molecules. Substituting this expression into equation (A 2), one obtains

$$\begin{aligned} I^{\mathrm{DA}}_{\mathrm{D,\,noFRET}} &= \left(\frac{B^{\mathrm{D}}_{\mathrm{D}} I_{\mathrm{ex,D}} \Gamma^{\mathrm{D}}_{\mathrm{D}}}{c}\right) Q_{\mathrm{D}}\psi^{\mathrm{A}}_{\mathrm{D}}((1-E)N^*_{\mathrm{D}} + N_{\mathrm{D}}) \\ &\quad + \left(\frac{B^{\mathrm{D}}_{\mathrm{D}} I_{\mathrm{ex,D}} \Gamma^{\mathrm{D}}_{\mathrm{D}}}{c}\right) Q_{\mathrm{D}}\psi^{\mathrm{A}}_{\mathrm{D}} N^*_{\mathrm{D}} E. \end{aligned} \tag{A 7}$$

The first term on the right-hand side of equation (A 7) can be identified as the fluorescence signal in the acceptor channel of the non-interacting donor, i.e. it is the donor bleed-through signal I^{DD} DER as given in equation (3.2). The second term can be identified from equation (A 3) to be equal to cFRETα. Hence equation (A 4) becomes

$$\mathrm{dFRET} = \frac{\mathrm{cFRET}\alpha}{I^{\mathrm{DD}}\mathrm{DER} + \mathrm{cFRET}\alpha}, \tag{A 8}$$

which is equation (4.2), as required.

Finally, the signal collection factors appearing in equation (A 5) can be written as

$$\psi = \frac{\Omega}{4\pi}\, Tg, \tag{A 9}$$

where Ω is the collection solid angle of detection optics; T is the fraction of photons transmitted through the system, which depends on the emission spectrum of the fluorophores, detection bandpass, etc.; and g is the detector gain. This means that

$$\frac{\psi^{\mathrm{A}}_{\mathrm{D}}}{\psi^{\mathrm{A}}_{\mathrm{A}}} = \frac{T^{\mathrm{A}}_{\mathrm{D}}}{T^{\mathrm{A}}_{\mathrm{A}}}, \tag{A 10}$$

and hence (A 5) becomes equation (4.3) and α is detector gain independent.

A.2. Derivation of aFRET

The signal in the detected acceptor channel on excitation at the acceptor channel in a system is given by

$$I^{\mathrm{AA}}_{\mathrm{A,\,noFRET}} = \left(\frac{B^{\mathrm{A}}_{\mathrm{A}} I_{\mathrm{ex,A}} \Gamma^{\mathrm{A}}_{\mathrm{A}}}{c}\right)(N_{\mathrm{A}} + N^*_{\mathrm{A}})\, Q_{\mathrm{A}}\psi^{\mathrm{A}}_{\mathrm{A}}. \tag{A 11}$$

Table A1. Terminology used in theoretical sections of the paper.

E	FRET efficiency, ranging from 0 to 100%
N_X	number of non-interacting fluorophores, species X
N_X^*	number of interacting fluorophores, species X
I^{DA}	signal upon excitation at the donor wavelength, detection by acceptor emission channel
I^{AA}	signal upon excitation at the donor wavelength, detection by acceptor emission channel
I^{DD}	signal upon excitation at the donor wavelength, detection by donor emission channel
I_D^{XY}	quantity refers to signal contribution from donor molecules, when excited at X and detected in Y
I_A^{XY}	quantity refers to signal contribution from acceptor molecules, when excited at X and detected in Y
$I_{ex,X}$	excitation irradiance per unit frequency interval, chosen to predominantly excite fluorophore X
cFRET	FRET signal corrected for signal crosstalk
dFRET	donor-concentration-normalized FRET efficiency
aFRET	acceptor-concentration-normalized FRET efficiency
AER	acceptor–excitation ratio, determines direct acceptor excitation at $I_{ex,D}$
DER	donor–emission ratio, determines bleed-through of donor emission into acceptor channel
α	normalization parameter for dFRET
β	normalization parameter for aFRET
Q_D	quantum yield of donor
Q_A	quantum yield of acceptor
T_D^A	collection efficiency for donor photons emitted into acceptor channel
T_A^A	collection efficiency for acceptor photons emitted into acceptor channel
ψ_X^Y	collection efficiency for signal from species X in detection channel Y
B_X^Y	Einstein B coefficient for stimulated absorption of species X at excitation wavelength Y
Γ_X^Y	spectral overlap factor of X at excitation wavelength Y
$XmYx$	the image collected in channel X when using excitation wavelength Y

Because there is no cross-excitation of the donor at the acceptor excitation wavelength, this equation can be rewritten as

$$I^{AA}_{A,\,noFRET} = I^{AA}, \tag{A 12}$$

where I^{AA} is defined as presented in §3.1.

Dividing equation (A 3) with equation (A 11), one obtains

$$\frac{N_D^*}{N_A + N_A^*} E = \frac{cFRET}{I_{AA}} \frac{B_A^A I_{ex,A} \Gamma_A^A}{B_D^D I_{ex,D} \Gamma_D^D}. \tag{A 13}$$

Now the AER was defined in equation (3.1) and in figure 4*a* and one can see that

$$AER = \frac{I^{DA}}{I^{AA}} = \frac{B_A^D I_{ex,D} \Gamma_A^D}{B_A^A I_{ex,A} \Gamma_A^A}. \tag{A 14}$$

On substitution of this into equation (A 13) and defining

$$\beta = \frac{B_D^D \Gamma_D^D}{B_A^D \Gamma_A^D}, \tag{A 15}$$

we obtain

$$aFRET = \frac{cFRET}{I_{AA} \beta AER}, \tag{A 16}$$

which is equation (4.5) as required.

A.3. FRET quantification by acceptor photobleaching

Acceptor photobleaching can also be used to quantify the FRET signal by measuring the increase in donor emission following photobleaching of the acceptor. The acceptor photobleaching technique is a calibration-free method for the determination of the transfer efficiency.

As mentioned previously, there is no direct excitation of the donor at the acceptor excitation wavelength, hence the signal I^{AA} is solely due to acceptors. Therefore, the relative change in I^{AA} after the photobleaching step represents the percentage P_B of acceptors that were photobleached. The signal detected in the donor channel before photobleaching upon excitation at the donor excitation wavelength is given by

$$I^{DD} = \left(\frac{B_D^D I_{ex,D} \Gamma_D^D}{c}\right)(N_D + N_D^*(1-E))\left(Q_D \psi_D^D\right). \tag{A 17}$$

The signal after photobleaching is given by

$$I^{DD}_{AB} = \left(\frac{B_D^D I_{ex,D} \Gamma_D^D}{c}\right)(N_D + N_D^*(1-E)(1-P_B) + N_D^* P_B)\left(Q_D \psi_D^D\right), \tag{A 18}$$

where P_B is the percentage of acceptors photobleached. Combining equations (A 17) and (A 18) gives

$$\frac{N_D^*}{N_D^* + N_D} E = \frac{1 - \frac{I^{DD}}{I^{DD}_{AB}}}{1 - \frac{I^{DD}}{I^{DD}_{AB}}(1 - P_B)}, \tag{A 19}$$

which is equation (4.14).

A.4. Software implementation

Software was written in interactive data language (RSI, Inc.) to implement the methodology developed here with an easy to use, intuitive user interface. The software is freely available from http://laser.ceb.cam.ac.uk/.

The program incorporates all features presented here for FRET quantification. Some of the more important features are as follows.

(i) The program uses the TIF file format for images, which all commercial microscopes can produce as output.
(ii) The sensitivity factors α and β can be calculated for a given excitation wavelength, detection bandpass and fluorophore type.
(iii) The AER and DER can be treated as constants, or allowed to vary as functions of intensity, either averaged over whole images or within user-selected regions of interest (ROIs). This has useful diagnostic value as explained in §3.2.
(iv) Background correction can be performed by subtracting the mean of a user-selected background region (e.g. a background obtained from a region containing no cells).
(v) Image thresholding can be performed by setting a minimum count level to be considered for analysis.
(vi) The image can be smoothed using a boxcar average smoothing function.
(vii) The level of corrected FRET, cFRET, can be calculated.
(viii) The donor- and acceptor-normalized FRET measurements, dFRET and aFRET, can be calculated.
(ix) If before- and after-photobleaching measurements are available, then the photobleaching technique can be used to calculate the level of FRET.
(x) The images can be analysed in terms of the mean, peak and standard deviation within a user-selected ROI.
(xi) Histograms of the image intensity or FRET level within a user-selected ROI can be displayed.
(xii) Intensity-overlay false-colour FRET images can be output as TIF files. In an intensity-overlay FRET image, the colour represents the level of FRET and the brightness represents the fluorescence intensity. This allows both intensity of emission and FRET level to be presented in one image.

A.5. Nomenclature

The nomenclature used in the theoretical sections of this paper is shown in table A1. In what follows, the symbols X and Y are placeholders for D and A. Superscripts are ordered with the first symbol denoting the excitation wavelength and the second symbol denoting the detection channel. Subscripts refer to signals from a particular species. For example, I^{DA} is the signal in the acceptor channel upon donor excitation; $I_{\mathrm{D}}^{\mathrm{DA}}$ is the signal in the acceptor channel upon donor excitation, which is due to donor molecules.

REFERENCES

Berney, C. & Danuser, G. 2003 FRET or no FRET: a quantitative comparison. *Biophys. J.* **84**, 3992–4010.

Calleja, V., Ameer-Beg, S. M., Vojnovic, B., Woscholski, R., Downward, J. & Larijani, B. 2003 Monitoring conformational changes of proteins in cells by fluorescence lifetime imaging microscopy. *Biochem. J.* **372**, 33–40. (doi:10.1042/BJ20030358)

Cario, G. & Franck, J. 1922 Über zerlegung von wasserstoffmolekülen durch angeregte quecksilberatome. *Z. Phys.* **11**, 161–166. (doi:10.1007/BF01328410)

Chan, F. K., Siegel, R. M., Zacharias, D., Swofford, R., Holmes, K. L., Tsien, R. Y. & Lenardo, M. J. 2001 Fluorescence resonance energy transfer analysis of cell surface receptor interactions and signaling using spectral variants of the green fluorescent protein. *Cytometry* **44**, 361–368. (doi:10.1002/1097-0320(20010801)44:4<361::AID-CYTO1128>3.0.CO;2-3)

Clayton, A. H. A., Hanley, Q. S. & Verveer, P. J. 2004 Graphical representation and multicomponent analysis of single-frequency fluorescence lifetime imaging microscopy data. *J. Microsc.* **213**, 1–5. (doi:10.1111/j.1365-2818.2004.01265.x)

Clegg, R. 1995 Fluorescence resonance energy transfer. *Curr. Opin. Biotechnol.* **6**, 103–110. (doi:10.1016/0958-1669(95)80016-6)

Clegg, R. 1996 *Fluorescence imaging spectroscopy and microscopy*. New York, NY: Wiley.

Digman, M., Caiolfa, V., Zamai, M. & Gratton, E. 2008 The phasor approach to fluorescence lifetime imaging analysis. *Biophys. J.* **94**, L14. (doi:10.1529/biophysj.107.120154)

Duncan, R. R., Bergmann, A., Cousin, M. A., Apps, D. K. & Shipston, M. J. 2004 Multi-dimensional time-correlated single photon counting (TCSPC) fluorescence lifetime imaging microscopy (FLIM) to detect fret in cells. *J. Microsc.* **215**, 1–12. (doi:10.1111/j.0022-2720.2004.01343.x)

Elangovan, M., Wallrabe, H., Chen, Y., Day, R. N., Barroso, M. & Periasamy, A. 2003 Characterization of one- and two-photon excitation fluorescence resonance energy transfer microscopy. *Methods J.* **29**, 58–73. (doi:10.1016/S1046-2023(02)00283-9)

Erickson, M., Alseikhan, B., Peterson, B. & Yue, D. 2001 Preassociation of calmodulin with voltage-gated Ca^{2+} channels revealed by FRET in single living cells. *Neuron* **31**, 973–985. (doi:10.1016/S0896-6273(01)00438-X)

Förster, T. 1948*a* Intermolecular energy migration and fluorescence. *Ann. Phys.* **2**, 55–75. (doi:10.1002/andp.19484370105)

Förster, T. 1948*b* Zwischenmolekulare energiewanderung und fluoreszenz. *Ann. Phys.* **437**, 55–75. (doi:10.1002/andp.19484370105)

Frank, J. H., Elder, A. D., Swartling, J., Venkitaraman, A. R., Jeyasekharan, A. D. & Kaminski, C. F. 2007 A white light confocal microscope for spectrally resolved multidimensional imaging. *J. Microsc.* **227**, 203–215. (doi:10.1111/j.1365-2818.2007.01803.x)

Gadella, T. & Jovin, T. M. 1995 Oligomerization of epidermal growth factor receptors on A431 cells studied by time-resolved fluorescence imaging microscopy. A stereochemical model for tyrosine kinase receptor activation. *J. Cell Biol.* **129**, 1543–1558. (doi:10.1083/jcb.129.6.1543)

Giepmans, B. N. G., Adams, S. R., Ellisman, M. H. & Tsien, R. Y. 2006 The fluorescence toolbox for assessing protein location and function. *Science* **312**, 217–224. (doi:10.1126/science.1124618)

Gordon, G. W., Berry, G., Liang, X. H., Levine, B. & Herman, B. 1998 Quantitative fluorescence resonance energy transfer measurements using fluorescence microscopy. *Biophys. J.* **74**, 2702–2713.

Grailhe, R., Merola, F., Ridard, J., Couvignou, S., Poupon, C. L., Changeux, J. & Laguitton-Pasquier, H. 2006 Monitoring protein interactions in the living cell through the fluorescence decays of the cyan fluorescent protein. *ChemPhysChem* **7**, 1442–1454. (doi:10.1002/cphc.200600057)

Gu, Y., Di, W. L., Kelsell, D. P. & Zicha, D. 2004 Quantitative fluorescence resonance energy transfer (FRET) measurement with acceptor photobleaching and spectral unmixing. *J. Microsc.* **215**, 162–173. (doi:10.1111/j.0022-2720.2004.01365.x)

Haj, F. G., Verveer, P. J., Squire, A., Neel, B. G. & Bastiaens, P. I. H. 2002 Imaging sites of receptor dephosphorylation by PTP1B on the surface of the endoplasmic reticulum. *Science* **295**, 1708–1711. (doi:10.1126/science.1067566)

Harpur, A. G., Wouters, F. S. & Bastiaens, P. I. H. 2001 Imaging FRET between spectrally similar GFP molecules in single cells. *Nat. Biotechnol.* **19**, 167–169. (doi:10.1038/84443)

Hoppe, A., Christensen, K. & Swanson, J. A. 2002 Fluorescence resonance energy transfer-based stoichiometry in living cells. *Biophys. J.* **83**, 3652–3664.

Jares-Erijman, E. A. & Jovin, T. M. 2003 FRET imaging. *Nat. Biotechnol.* **21**, 1387–1395. (doi:10.1038/nbt896)

Jares-Erijman, E. A. & Jovin, T. M. 2006 Imaging molecular interactions in living cells by FRET microscopy. *Curr. Opin. Chem. Biol.* **10**, 409–416. (doi:10.1016/j.cbpa.2006.08.021)

Jiang, X. & Sorkin, A. 2002 Coordinated traffic of Grb2 and Ras during epidermal growth factor receptor endocytosis visualized in living cells. *Mol. Biol. Cell* **13**, 1522–1535. (doi:10.1091/mbc.01-11-0552)

Kenworthy, A. K. 2001 Imaging protein–protein interactions using fluorescence resonance energy transfer microscopy. *Methods* **24**, 289–296. (doi:10.1006/meth.2001.1189)

Kobayashi, H., Stewart, E., Poon, R., Adamczewski, J. P., Gannon, J. & Hunt, T. 1992 Identification of the domains in cyclin are required for binding to, and activation of, p34cdc2 and p32cdk2 protein kinase subunits. *Mol. Biol. Cell* **3**, 1279–1294.

Kölner, M. & Wolfrum, J. 1992 How many photons are necessary for fluorescence lifetime measurements? *Chem. Phys. Lett.* **200**, 199–204. (doi:10.1016/0009-2614(92)87068-Z)

Lakowicz, J. R. 1999 *Principles of fluorescence spectroscopy*, 2nd edn. New York, NY: Plenum Press.

Lakowicz, J. R. 2006 *Principles of fluorescence spectroscopy*, 3rd edn. Berlin, Germany: Springer.

Llopis, J. *et al.* 2000 Ligand-dependent interactions of coactivators steroid receptor coactivator-1 and peroxisome proliferator-activated receptor binding protein with nuclear hormone receptors can be imaged in live cells and are required for transcription. *Proc. Natl Acad. Sci. USA* **97**, 4363–4368. (doi:10.1073/pnas.97.8.4363)

Mekler, V. M. 1994 A photochemical technique to enhance sensitivity of detection of fluorescence resonance energy-transfer. *Photochem. Photobiol.* **59**, 615–620. (doi:10.1111/j.1751-1097.1994.tb08227.x)

Mekler, V., Averbakh, A., Sudarikov, A. & Kharitonova, O. 1997 Fluorescence energy transfer-sensitized photobleaching of a fluorescent label as a tool to study donor–acceptor distance distributions and dynamics in protein assemblies: studies of a complex of biotinylated IgM with streptavidin and aggregates of concanavalin A. *J. Photochem. Photobiol. B: Biol.* **40**, 278–287. (doi:10.1016/S1011-1344(97)00070-5)

Millington, M. *et al.* 2007 High-precision FLIM–FRET in fixed and living cells reveals heterogeneity in a simple CFP–YFP fusion protein. *Biophys. Chem.* **127**, 155–164. (doi:10.1016/j.bpc.2007.01.008)

Miyawaki, A. 2003 Visualization of the spatial and temporal dynamics of intracellular signaling. *Dev. Cell* **4**, 295–305. (doi:10.1016/S1534-5807(03)00060-1)

Morgan, D. O. 2007 *The cell cycle: principles of control*. Oxford, UK: Oxford University Press.

Nagy, P., Vamosi, G., Bodnar, A., Lockett, S. J. & Szollosi, J. 1998 Intensity-based energy transfer measurements in digital imaging microscopy. *Eur. Biophys. J.* **27**, 377–389. (doi:10.1007/s002490050145)

Neher, R. & Neher, E. 2004*a* Applying spectral fingerprinting to the analysis of FRET images. *J. Microsc. Res. Tech.* **64**, 185–195. (doi:10.1002/jemt.20078)

Neher, R. & Neher, E. 2004*b* Optimizing imaging parameters for the separation of multiple labels in a fluorescence image. *J. Microsc.* **213**, 46–62. (doi:10.1111/j.1365-2818.2004.01262.x)

Ng, T. *et al.* 1999 Imaging protein kinase Calpha activation in cells. *Science* **283**, 2085–2089. (doi:10.1126/science.283.5410.2085)

Pelet, S., Previte, M., Laiho, L. & So, P. 2004 A fast global fitting algorithm for fluorescence lifetime imaging microscopy based on image segmentation. *Biophys. J.* **87**, 2807–2817. (doi:10.1529/biophysj.104.045492)

Periasamy, A. & Day, R. N. (eds) 2005 *Molecular imaging: FRET microscopy and spectroscopy*. Oxford, UK: Oxford University Press.

Perrin, F. 1932 Theorie quantique des transferts deactivation entre molecules de meme espece: cas des solutions fluorescents. *Ann. Phys.* (*Paris*) **12**, 283–314.

Perrin, J. 1927 Fluorescence and molecular induction by resonance. *CR Acad. Sci. Paris* **184**, 1097–1100.

Pollok, B. & Heim, R. 1999 Using GFP in FRET-based applications. *Trends Cell Biol.* **9**, 57–60. (doi:10.1016/S0962-8924(98)01434-2)

Rizzo, M. & Piston, D. 2005 High-contrast imaging of fluorescent protein FRET by fluorescence polarization microscopy. *Biophys. J.* **88**, 14–16. (doi:10.1529/biophysj.104.055442)

Rizzo, M. A., Springer, G. H., Granada, B. & Piston, D. W. 2004 An improved cyan fluorescent protein variant useful for FRET. *Nat. Biotechnol.* **22**, 445–449. (doi:10.1038/nbt945)

Russo, A. A., Jeffrey, P. D. & Pavletich, N. P. 1996 Structural basis of cyclin-dependant kinase activation by phosphorylation. *Nat. Struct. Biol.* **3**, 696–700. (doi:10.1038/nsb0896-696)

Selvin, P. 2000 The renaissance of fluorescence resonance energy transfer. *Nat. Struct. Biol.* **7**, 730–734. (doi:10.1038/78948)

Shaner, N. C., Steinbach, P. A. & Tsien, R. Y. 2005 A guide to choosing fluorescent proteins. *Nat. Methods* **2**, 905–909. (doi:10.1038/nmeth819)

Shu, X., Shaner, N., Yarbrough, C., Tsien, R. & Remington, S. 2006 Novel chromophores and buried charges control colour in mfruits. *Biochemistry* **45**, 9639–9647. (doi:10.1021/bi060773l)

Stryer, L. 1978 Fluorescence energy transfer as a spectroscopic ruler. *Annu. Rev. Biochem.* **47**, 819–846. (doi:10.1146/annurev.bi.47.070178.004131)

Tramier, M., Gautier, I., Piolot, T., Ravalet, S., Kemnitz, K., Coppey, J., Durieux, C., Mignotte, V. & Coppey-Moisan, M. 2002 Picosecond-hetero-fret microscopy to probe protein–protein interactions in live cells. *Biophys. J.* **83**, 3570–3577.

Tron, L., Szollosi, J., Damjanovich, S., Helliwell, S., Arndt-Jovin, D. & Jovin, T. 1984 Flow cytometric measurement

of fluorescence resonance energy transfer on cell surfaces. Quantitative evaluation of the transfer efficiency on a cell-by-cell basis. *Biophys. J.* **45**, 939–946.

Valentin, G., Verheggen, C., Piolot, T., Neel, H., Coppey-Moisan, M. & Bertrand, E. 2005 Photoconversion of YFP into a CFP-like species during acceptor photobleaching FRET experiments. *Nat. Methods* **2**, 801. (doi:10.1038/nmeth1105-801)

Vanderklish, P. W., Krushel, L. A., Holst, B. H., Gally, J. A., Crossin, K. L. & Edelman, G. M. 2000 Marking synaptic activity in dendritic spines with a calpain substrate exhibiting fluorescence resonance energy transfer. *Proc. Natl Acad. Sci. USA* **97**, 2253–2258. (doi:10.1073/pnas.040565597)

Van Der Meer, B. 2002 Kappa-squared: from nuisance to new sense. *Rev. Mol. Biotechnol.* **82**, 181–196. (doi:10.1016/S1389-0352(01)00037-X)

Van Munster, E. B., Kremers, G. J., Adjobo-Hermans, M. J. W. & Gadella, T. W. J. 2005 Fluorescence resonance energy transfer (FRET) measurement by gradual acceptor photobleaching. *J. Microsc.* **218**, 253–262. (doi:10.1111/j.1365-2818.2005.01483.x)

Van Rheenen, J., Langeslag, M. & Jalink, K. 2004 Correcting confocal acquisition to optimize imaging of fluorescence resonance energy transfer by sensitized emission. *Biophys. J.* **86**, 2517–2529.

Verveer, P., Wouters, F., Reynolds, A. & Bastiaens, P. I. H. 2000 Quantitative imaging of lateral ErbB1 receptor signal propagation in the plasma membrane. *Science* **290**, 1567–1570. (doi:10.1126/science.290.5496.1567)

Wallrabe, H. & Periasamy, A. 2005 Imaging protein molecules using FRET and FLIM microscopy. *Curr. Opin. Biotechnol.* **16**, 19–27. (doi:10.1016/j.copbio.2004.12.002)

Wlodarczyk, J., Woehler, A., Kobe, F., Ponimaskin, E., Zeug, A. & Neher, E. 2008 Analysis of fret signals in the presence of free donors and acceptors. *Biophys. J.* **94**, 986–1000. (doi:10.1529/biophysj.107.111773)

Wouters, F. S., Bastiaens, P. I., Wirtz, K. W. & Jovin, T. M. 1998 FRET microscopy demonstrates molecular association of non-specific lipid transfer protein (nsL-TP) with fatty acid oxidation enzymes in peroxisomes. *EMBO J.* **17**, 7179–7189. (doi:10.1093/emboj/17.24.7179)

Wouters, F. S., Verveer, P. & Bastiaens, P. 2001 Imaging biochemistry inside cells. *Trends Cell Biol.* **11**, 203–211. (doi:10.1016/S0962-8924(01)01982-1)

Xia, Z. & Liu, Y. 2001 Reliable and global measurement of fluorescence resonance energy transfer using fluorescence microscopes. *Biophys. J.* **81**, 2395–2402.

Youvan, D. C., Silva, C. M., Bylina, E. J., Coleman, W. J., Dilworth, M. R. & Yang, M. M. 1997 Calibration of fluorescence resonance energy transfer in microscopy using genetically engineered GFP derivatives on nickel chelating beads. *Biotechnology* **3**, 1–18.

Zal, T. & Gascoigne, N. R. J. 2004 Photobleaching-corrected FRET efficiency imaging of live cells. *Biophys. J.* **86**, 3923–3939. (doi:10.1529/biophysj.103.022087)